The carboxyl-terminal region of SDCCAG8 comprises a functional module essential for cilia formation as well as organ development and homeostasis

SDCCAG8 の C 末端領域は繊毛形成ならびに器官の発生と恒常性に必要不可欠な機能的モジュールを構成する

大阪大学 理学研究科 生物科学専攻

分子発生学研究室

(PI: 古川 貴久 教授)

堤 崚太郎

Abstract

Cilia are microtubule-based organelles that serve a variety of sensory and motile functions across different species. Ciliary dysfunction in humans causes “ciliopathies”, which can present with a broad spectrum of symptoms, including developmental and sensory abnormalities. We previously reported that intestinal cell kinase (Ick), also known as ciliogenesis-associated kinase 1 (Cilk1), and male germ cell-associated kinase (Mak) regulate ciliary protein trafficking and cilia length in mammals. Mutations in the *ICK* and *MAK* genes lead to ciliopathies with multiple developmental defects and retinitis pigmentosa, respectively. Although many gene mutations associated with ciliopathies have been identified, the molecular and pathological mechanisms underlying ciliopathies are not well understood.

To address these issues, we screened and found that Ick and Mak interact with serologically defined colon cancer antigen 8 (Sdccag8), a centrosomal/basal body protein essential for cilia formation and Hedgehog signaling. The *SDCCAG8* gene mutations are associated with ciliopathies with multiple organ defects, including hypogonadism. In addition, we narrowed down the Ick- and Mak- interacting module to the carboxyl (C)-terminal region of Sdccag8 (Sdccag8-C). Notably, several mutations are predicted to truncate the SDCCAG8 C-terminus in humans. *In vitro* experiments using cultured cells showed that Sdccag8-C is required for Sdccag8 localization to centrosomes and cilia formation. To analyze the roles of Sdccag8-C *in vivo*, we generated mice in which Sdccag8-C was truncated (*Sdccag8*$^{\Delta C/\Delta C}$ mice) using the CRISPR-mediated stop codon knock-in strategy. We observed the weak localization of Sdccag8 to centrosomes and/or basal bodies in *Sdccag8*$^{\Delta C/\Delta C}$ MEFs and retinal photoreceptor cells. In addition, we observed abnormalities in cilia formation and Hedgehog signaling, and ciliopathy-like

organ defects, including cleft palate, polydactyly, and retinal and renal degeneration in *Sdccag8*$^{\Delta C/\Delta C}$ mice. These phenotypes observed in the *Sdccag8*$^{\Delta C/\Delta C}$ mice partially overlapped with those previously observed in *Ick*- and *Mak*-deficient mice. Furthermore, *Sdccag8*$^{\Delta C/\Delta C}$ mice showed spermatogenesis defects, which are a previously uncharacterized phenotype resulting from Sdccag8 dysfunction.

Collectively, our results suggest that Sdccag8-C is an Ick and Mak-interacting module that is required for the localization of Sdccag8 to centrosomes/basal bodies. In addition, Sdccag8-C is essential for cilia formation and thereby for organ development and homeostasis. The current findings shed light on the molecular and pathological mechanisms underlying the ciliopathies observed in patients with *SDCCAG8* mutations, and may advance our understanding of protein-protein interaction networks involved in cilia development.

Table of Contents

Introduction

Cilia are evolutionarily conserved microtubule-based organelles that extend from the basal bodies and are formed on the cell surface (Gerdes et al., 2009; Malicki and Johnson, 2017). They are generally classified into two categories: motile cilia and primary cilia (Ishikawa and Marshall, 2011). Motile cilia are formed on specific epithelial cell types and cooperatively beat in wave-like patterns to generate fluid flow. Sperm flagella are an example of motile cilia which mainly function in cell locomotion. On the other hand, primary cilia are present in almost every cell type in vertebrates and act as cellular antennae to sense physical and biochemical extracellular signals. In humans, ciliary dysfunction causes diseases known as ciliopathies, which are characterized by a broad spectrum of pathologies, including polydactyly, craniofacial abnormalities, brain malformation, situs inversus, obesity, diabetes, retinal and renal degeneration, hearing loss, and infertility (Nigg and Raff, 2009; Hildebrandt et al., 2011).

Many ciliary proteins are known to play important roles in human physiology, cell signaling, and development (Reiter and Leroux, 2017). It was recently reported that there are at least 38 established ciliopathies with mutations in at least 247 genes (Lovera and Luders, 2021). For example, Bardet-Biedl syndrome (BBS), which is an autosomal recessive ciliopathy that results in a plethora of developmental and multiorgan defects, is known to be caused by mutations in 22 identified pathogenic genes (McConnachie et al., 2021). In addition, mutations in more than 25 different pathogenic genes have been shown to be associated with nephronophthisis (NPHP), an autosomal recessive renal ciliopathy with additional features such as retinal defects, liver fibrosis, skeletal abnormalities, and brain developmental disorders (Luo and Tao, 2018). Although many gene mutations

causing ciliopathies have been found in humans, the molecular and pathological mechanisms underlying ciliopathies are still not well understood.

Serologically defined colon cancer antigen 8 (SDCCAG8) was identified as a centrosome-associated tumor antigen protein and is also known as centrosomal colon cancer autoantigen protein (CCCAP), NPHP10, and BBS16 (Kenedy et al., 2003). Mutations in the human *SDCCAG8* gene are associated with an NPHP-related ciliopathy, characterized by retinal and renal degeneration, cognitive defects, obesity, hypogonadism, hearing loss, recurrent respiratory infections, and infrequently clinodactyly (Otto et al., 2010; Schaefer et al., 2011; Billingsley et al., 2012; Yamamura et al., 2017; Watanabe et al., 2019; Bahmanpour et al., 2021). Several studies have reported that Sdccag8 is required for cilia formation and Hedgehog signaling (Insolera et al., 2014; Airik et al., 2016; Flynn et al., 2020). *Sdccag8* knockout mice mostly died after birth with multiple organ defects, and *Sdccag8* gene-trap mice exhibited retinal and renal degeneration (Airik et al., 2014; Insolera et al., 2014). It has also been reported that Sdccag8 is associated with the regulation of pericentriolar material (PCM) recruitment (Insolera et al., 2014). Several mutations in the human *SDCCAG8* gene that are predicted to truncate the Sdccag8 carboxyl (C)-terminus are associated with multiple organ defects, including retinal degeneration and cystic kidney (Otto et al., 2010; Schaefer et al., 2011; Billingsley et al., 2012); however, the underlying pathological mechanisms are poorly understood.

We and others have previously reported that intestinal cell kinase (Ick), also known as ciliogenesis-associated kinase 1 (Cilk1), and male germ cell-associated kinase (Mak) play crucial roles in the regulation of cilia length and ciliary transport in mammals (Omori et al., 2010; Broekhuis et al., 2014; Chaya et al., 2014; Moon et al., 2014; Okamoto et al., 2017; Chaya and Furukawa, 2021). Ick and Mak are evolutionarily conserved serine-

threonine kinases that belong to the mitogen-activating protein kinase family and show high homology to each other, especially in their catalytic domains (Figs. 1A and B) (Miyata and Nishida, 1999; Togawa et al., 2000; Shinkai et al., 2002). Several missense mutations in the human *ICK* gene have been reported to lead to endocrine-cerebro-osteodysplasia (ECO) syndrome or short-rib polydactyly syndrome (SRPS), lethal recessive ciliopathies with multiple developmental abnormalities, including cleft palate and cystic kidneys (Lahiry et al., 2009; Oud et al., 2016; Paige Taylor et al., 2016). Mutations in the human *MAK* gene also cause autosomal recessive retinitis pigmentosa (Ozgul et al., 2011; Tucker et al., 2011).

To elucidate the molecular and pathological mechanisms underlying ciliopathies, we screened and found that Ick and Mak interact with the C-terminal region of Sdccag8 (Sdccag8-C), and investigated the role of Sdccag8-C *in vitro* and *in vivo* in the current study. *In vitro* experiments using cultured cells showed that Sdccag8-C is required for Sdccag8 localization to centrosomes and cilia formation. We then generated a mouse mutant in which Sdccag8-C was truncated (*Sdccag8*$^{\Delta C/\Delta C}$ mice) using the CRISPR-mediated stop codon knock-in strategy. In *Sdccag8*$^{\Delta C/\Delta C}$ mice, we observed abnormalities in cilia formation and ciliopathy-like organ phenotypes, which partially overlapped with those previously observed in *Ick*- and *Mak*-deficient mice. Together, these results shed light on the molecular and pathological mechanisms underlying the ciliopathies observed in patients with *SDCCAG8* mutations, and may advance our understanding of the ciliopathy protein-protein interaction network.

Results

Ick expression is enriched in the retina, brain, lung, intestine, and reproductive system

To investigate the molecular mechanisms of cilia development and ciliopathies, I first performed reverse transcription-polymerase chain reaction (RT-PCR) analysis of *Ick* and *Mak* using various mouse tissue cDNAs at 4 weeks old (wks) (Fig. 1C). I observed that *Ick* is ubiquitously expressed in various tissues, whereas the *Mak* expression was highly enriched in the retina and testis. Among tissues, the *Ick* signal was relatively strong in the retina, brain, lung, intestine, and reproductive system. In the following analysis, we focused on the brain, testis, and intestine, in which the *Ick* expression pattern has not been well characterized at the adult stage.

Ick is expressed in brain regions where proliferating cells are localized

To investigate the *Ick* expression in the adult brain, I carried out *in situ* hybridization analysis using 4 wks coronal brain sections (Figs. 2A-J). I observed that *Ick* is expressed in the lateral ventricle (Fig. 2A), hippocampus (Fig. 2B), piriform cortex (Fig. 2B), and cerebellum (Fig. 2C). Among them, the *Ick* signal was relatively strong in the lateral ventricle. I observed that *Ick* is expressed throughout the lateral walls, especially in the dorsal edge and ventral tip of the lateral walls (Figs. 2D and E). In mammals, the ventricular-subventricular zone (V-SVZ) on the walls of the lateral ventricle retains neural stem cells. Neural precursor cells generated from the V-SVZ proliferate, differentiate, and migrate along the rostral migratory stream (RMS), and subsequently are integrated into the olfactory bulb as interneurons (Lois and Alvarez-Buylla, 1994; Ming and Song, 2011;

Fuentealba et al., 2015). *Ick* expression was observed in the RMS of the olfactory bulb in addition to the lateral ventricle (Figs. 2F-H). Adult neurogenesis also occurs in the subgranular zone (SGZ) of the hippocampal dentate gyrus (DG) (van Praag et al., 2002; Ming and Song, 2011). I observed *Ick* signals in the DG, especially in the SGZ (Figs. 2I and J). These results suggest that *Ick* is expressed in brain regions in which cell proliferation can be observed at the adult stage.

Ick is expressed in spermatocytes and spermatids in the adult testis

To examine the *Ick* expression in the testis, I performed *in situ* hybridization analysis on mature mouse testis sections at 16 wks (Fig. 3A). I observed *Ick* signals in seminiferous tubules of the testis. I also performed *in situ* hybridization analysis using several cell-type markers; *Promyelocytic leukemia zinc-finger* (*PLZF*) as a spermatogonia marker (Fig. 3B), *Acrosin* (*Acr*) as a pachytene spermatocyte to round spermatid marker (Fig. 3C), *Calmegin* (*Clgn*) as a pachytene spermatocyte to spermatid marker (Fig. 3D), *3β-hydroxysteroid dehydrogenase/Δ5-Δ4 isomerase* (*3β-HSD*) as a Leydig cell marker (Fig. 3E), and *Sox9* as a Sertoli cell marker (Fig. 3F) (Mizuhashi et al., 2015). In the process of spermatogenesis, spermatogonia are sequentially differentiated into spermatocytes, spermatids, and spermatozoa (Cheng and Mruk, 2002). We found that the staining pattern of *Ick* is similar to that of *Acr* and *Clgn*. These results suggest that *Ick* transcripts are expressed in pachytene spermatocytes to spermatids in the mature testis.

Ick is expressed in intestinal stem cells

I examined the *Ick* expression in the adult small intestine at 8 wks by *in situ* hybridization together with several marker gene expressions (Figs. 4A-D). I used *Lgr5* as

a stem cell marker (Fig. 4B) (van der Flier et al., 2009), *Wnt3* as a Paneth cell marker (Fig. 4C) (Sato et al., 2011), and *Slc5a1* as an enterocyte marker (Fig 4D) (Gerbe et al., 2016). I observed that *Ick* is expressed in the intestinal crypt similar to *Lgr5* and *Wnt3* but not to *Slc5a1* (Figs. 4A-D). To identify *Ick*-expressing cell types in the crypt of the small intestine, I prepared the serial sections, performed *in situ* hybridization, and compared the *Ick* expression with the *Lgr5* and *Wnt3* expression patterns (Figs. 4E-I). I first observed the *Ick*, *Lgr5*, and *Wnt3* signals in each crypt. The staining patterns between *Ick* and *Lgr5* were more similar than those of *Ick* and *Wnt3* (Figs. 4E and F). In addition, I observed their expression patterns within a crypt where the *Ick* signal was detected together with *Lgr5* and/or *Wnt3* signals. We found that *Ick* and *Lgr5* signals are enriched and overlapped in the inside of crypt bottoms, whereas the *Wnt3* signal was broadly distributed (Figs. 4G-I). These results suggest that the *Ick* mRNA is expressed in intestinal stem cells. Collectively, our observations imply that *Ick* is expressed in proliferating regions in the adult mouse brain, testis, and intestine.

Ick and Mak interact with the C-terminal region of Sdccag8

We screened for proteins that interact with Ick protein using yeast two-hybrid screening, and identified various proteins, including Sdccag8 (Table 1). Since this protein has previously been associated with ciliopathies with multiple organ defects as well as ICK, we focused on Sdccag8 in the present study. First, I confirmed the interaction between Ick and Sdccag8 by immunoprecipitation assay using HEK293T cells with an anti-FLAG antibody (Fig. 5A). To confirm the endogenous interaction between Ick and Sdccag8, I performed an immunoprecipitation assay using a HEK293T cell extract with an anti-SDCCAG8 antibody (Fig. 5B). I observed the ICK band in immunoprecipitates

with the anti-SDCCAG8 antibody by western blot. This result suggests the endogenous interaction between ICK and SDCCAG8. The immunoprecipitation assay also revealed an interaction between Mak and Sdccag8 (Fig. 5A). Human SDCCAG8 is a ciliary protein that consists of eight predicted coiled-coil motifs and can be divided into three regions: amino (N)-terminal (1–294 aa), middle (286–541 aa), and C-terminal (533–713 aa, SDCCAG8-C) (Otto et al., 2010). To determine which region of Sdccag8 interacts with Ick and Mak, we divided mouse Sdccag8 into three regions (N-terminal (1–298 aa, Sdccag8-N), middle (290–545 aa, Sdccag8-M), and C-terminal (537–717 aa, Sdccag8-C)), and examined their interaction with Ick and Mak by immunoprecipitation assays (Fig. 5C). Immunoprecipitation assays showed that both Ick and Mak interacted with the full-length Sdccag8 (Sdccag8-FL) and Sdccag8-C, but not Sdccag8-N or Sdccag8-M (Figs. 5D and E). These results suggest that Ick and Mak interact with Sdccag8-C.

The C-terminal region is required for the localization of Sdccag8 to centrosomes

Since the Sdccag8 protein is known to localize to centrosomes and basal bodies (Kenedy et al., 2003; Otto et al., 2010), we analyzed the role of Sdccag8-C in localizing to centrosomes. I transfected the plasmids expressing FLAG-tagged enhanced green fluorescent protein (EGFP), Sdccag8-FL, Sdccag8-N, Sdccag8-M, the N-terminal to middle region of mouse Sdccag8 (1–545 aa, Sdccag8-NM), or Sdccag8-C into NIH-3T3 cells, and compared their localization to centrosomes by immunostaining with antibodies against FLAG and γ-tubulin (a marker for centrosomes and basal bodies). I observed that Sdccag8-FL and -C localize to centrosomes in NIH-3T3 cells, although the signal intensity of Sdccag8-C at centrosomes was lower than that of Sdccag8-FL (Fig. 6A). In contrast, signals of Sdccag8-N, -M, and -NM were not detected at centrosomes. These

results suggest that Sdccag8-C is required for localization to the basal bodies. To further analyze the localization of Sdccag8-C at basal bodies, I prepared the plasmids expressing a FLAG-tagged mouse Sdccag8-C1 (537–600 aa), -C2 (537–642 aa), -C3 (601–717 aa), or -C4 (643–717 aa), considering the evolutionary conservation of the amino acid sequences in vertebrate Sdccag8 proteins (Fig. 6B). I transfected plasmids expressing FLAG-tagged EGFP, Sdccag8-C, Sdccag8-C1, Sdccag8-C2, Sdccag8-C3, or Sdccag-C4 into NIH-3T3 cells and compared their localization to centrosomes. Unexpectedly, I did not observe signals corresponding Sdccag8-C1, -C2, -C3 and -C4 at centrosomes, whereas Sdccag8-C localized at centrosomes in NIH-3T3 cells (Fig. 6C). These results suggest that the entire Sdccag8-C (537–717 aa) comprises a functional unit that can localize to basal bodies.

The C-terminal region of Sdccag8 is required for cilia formation in cultured cells

To investigate the roles of Sdccag8-C in cilia formation, I performed knockdown and rescue experiments using NIH-3T3 cells. I first constructed short hairpin RNAs (shRNAs) to knockdown *Sdccag8* and confirmed that Sdccag8-shRNA2 and -shRNA3 suppressed the Sdccag8 expression (Fig. 7A). I transfected these constructs into NIH-3T3 cells and examined the cilia by immunostaining using anti-acetylated α-tubulin (a ciliary marker) and anti-FLAG antibodies. I observed that Sdccag8-shRNA2 and Sdccag8-shRNA3 significantly decreased the number of ciliated cells and cilia length (Figs. 7B-D). Next, we prepared plasmids expressing a FLAG-tagged full-length human SDCCAG8 (1–713 aa, hSDCCAG8-FL) and the N-terminal to middle region of human SDCCAG8 (1–541 aa, hSDCCAG8-NM). I transfected the shRNA-control or Sdccag8-shRNA3 expression plasmids with plasmids expressing FLAG-tagged EGFP, hSDCCAG8-FL, or

hSDCCAG8-NM into NIH-3T3 cells, and examined the cilia by immunostaining using anti-acetylated α-tubulin and anti-FLAG antibodies. We found that the expression of hSDCCAG8-FL rescued the Sdccag8-shRNA-induced inhibition of cilia formation (Figs. 7E-G). In contrast, the expression of hSDCCAG8-NM failed to rescue the Sdccag8-shRNA-induced inhibition of cilia formation. These results suggest that SDCCAG8-C is required for cilia formation.

Sdccag8 Arg537Stop knock-in mice show partial postnatal lethality and skeletal defects

Next, to examine the *in vivo* roles of Sdccag8-C, we generated *Sdccag8* Arg537Stop knock-in (*Sdccag8*$^{\Delta C/\Delta C}$) mice using CRISPR-Cas9 system. A stop codon and an EcoRI restriction site were knocked-in before the DNA sequence encoding Sdccag8-C (537–717 aa) in *Sdccag8*$^{\Delta C/\Delta C}$ mice (Fig. 8A). The EcoRI restriction site was inserted to facilitate the detection of the stop codon insertion (Fig. 8B). I carried out RT-PCR analysis and confirmed that the expression levels of *Sdccag8* mRNA were comparable between *Sdccag8*$^{+/+}$ and *Sdccag8*$^{\Delta C/\Delta C}$ mice (Fig. 8C), suggesting that *Sdccag8* mRNA is not degraded by nonsense-mediated decay in *Sdccag8*$^{\Delta C/\Delta C}$ mice.

To examine the survival of *Sdccag8*$^{\Delta C/\Delta C}$ mice, I measured the genotype distribution of the offspring from *Sdccag8*$^{\Delta C/+}$ parents at the neonatal stages from postnatal day 0 (P0) to P2 and at postnatal stages from P12 to 1 month old (1M). The survival ratio of *Sdccag8*$^{\Delta C/\Delta C}$ mice was approximately 2.5 times lower than that of *Sdccag8*$^{+/+}$ mice from P12 to 1M, whereas *Sdccag8*$^{\Delta C/\Delta C}$ mice were present at the expected Mendelian ratios at neonatal stages (Fig. 8D). This result suggests that *Sdccag8*$^{\Delta C/\Delta C}$ mice exhibit partial postnatal lethality, but not embryonic lethality. Furthermore, we found that one

Sdccag8$^{\Delta C/\Delta C}$ mouse showed a cleft palate (Fig. 8E). We also found that several *Sdccag8*$^{\Delta C/\Delta C}$ mice exhibited polydactyly (Fig. 8F). These observations suggest that Sdccag8-C is required for proper skeletal development.

The C-terminal region of Sdccag8 is essential for cilia formation and function in embryonic fibroblasts

Since *Sdccag8*$^{\Delta C/\Delta C}$ mice exhibited ciliopathy-like phenotypes such as cleft palate and polydactyly, we examined cilia formation and function in *Sdccag8*$^{\Delta C/\Delta C}$ mice. To investigate the role of Sdccag8-C in cilia formation and function, we analyzed cilia in mouse embryonic fibroblasts (MEFs) from *Sdccag8*$^{\Delta C/\Delta C}$ embryos. I first performed immunofluorescent analyses of *Sdccag8*$^{\Delta C/\Delta C}$ MEFs using antibodies against Sdccag8 and γ-tubulin. I observed that Sdccag8 signals at centrosomes in *Sdccag8*$^{\Delta C/\Delta C}$ MEFs were lower than those in *Sdccag8*$^{+/+}$ MEFs (Fig. 9A). In addition, I did not observe the signal of the isotype control at centrosomes in *Sdccag8*$^{\Delta C/\Delta C}$ MEFs (Fig. 9B). These results suggest a weak localization of Sdccag8 at centrosomes in *Sdccag8*$^{\Delta C/\Delta C}$ MEFs. I next performed immunofluorescent analyses of MEFs using the antibody against acetylated α-tubulin and found that the number of ciliated cells and cilia length significantly decreased in *Sdccag8*$^{\Delta C/\Delta C}$ MEFs compared with that in *Sdccag8*$^{+/+}$ MEFs (Figs. 9C-E). To examine whether the loss of Sdccag8-C affects intraflagellar transport (IFT), the bidirectional protein transport system in cilia, I immunostained IFT88 (a component of IFT complex) in the cilia of *Sdccag8*$^{\Delta C/\Delta C}$ MEFs. I observed no obvious difference in the ciliary localization of IFT88 between *Sdccag8*$^{+/+}$ and *Sdccag8*$^{\Delta C/\Delta C}$ MEFs (Fig. 9F). Cilia are known to play important roles in Hedgehog signal transduction (Huangfu and Anderson, 2005). To examine whether the loss of Sdccag8-C affects Hedgehog signaling, we first

observed Hedgehog signal-dependent ciliary localization of Smoothened (Smo), a Hedgehog signaling component, in *Sdccag8*$^{\Delta C/\Delta C}$ MEFs with or without treatment of a Smo agonist (SAG) (Chen et al., 2002). Activation of the Hedgehog pathway with SAG treatment induces ciliary localization of Smo (Rohatgi et al., 2007). We observed no significant difference in the Smo localization to cilia between *Sdccag8*$^{+/+}$ and *Sdccag8*$^{\Delta C/\Delta C}$ MEFs (Figs. 9G and H). We next examined the expression level of *Gli family zinc finger 1* (*Gli1*), a downstream target gene of the Hedgehog signaling cascade, in *Sdccag8*$^{\Delta C/\Delta C}$ MEFs by quantitative RT-PCR (qRT-PCR) analysis. The qRT-PCR analysis showed that *Gli1* expression significantly decreased in *Sdccag8*$^{\Delta C/\Delta C}$ MEFs compared with that in *Sdccag8*$^{+/+}$ MEFs in the presence of the Hedgehog pathway activation signals (Fig. 9I). These results suggest that Sdccag8-C plays an important role in cilia formation and the Hedgehog signal transduction.

Deficiency of the C-terminal region of Sdccag8 causes retinal degeneration

To examine the *Sdccag8* expression in various tissues, I performed RT-PCR analysis using mouse tissue cDNAs at 4 wks. RT-PCR analysis showed that *Sdccag8* as well as *Ick* is ubiquitously expressed in various tissues, including the retina, kidney, and testis (Fig. 10A). To examine *Sdccag8* expression in the retina, I performed *in situ* hybridization using retinal sections at P9. I observed that *Sdccag8* transcripts were broadly expressed in the retina (Fig. 10B).

To investigate the roles of Sdccag8-C in the retina, I carried out histological analyses using retinal sections from *Sdccag8*$^{+/+}$ and *Sdccag8*$^{\Delta C/\Delta C}$ mice. Toluidine blue staining showed that there was no significant difference between the *Sdccag8*$^{+/+}$ and *Sdccag8*$^{\Delta C/\Delta C}$ retinas at P14; however, the outer nuclear layer (ONL) thickness in the *Sdccag8*$^{\Delta C/\Delta C}$

retina progressively decreased after 6 wks (Figs. 10C and D). In contrast, I observed no significant difference in the thickness of the other layers between the *Sdccag8*$^{+/+}$ and *Sdccag8*$^{\Delta C/\Delta C}$ retinas (Fig. 10E). These results indicate that *Sdccag8*$^{\Delta C/\Delta C}$ mice exhibit progressive photoreceptor degeneration. To observe outer segments in the *Sdccag8*$^{\Delta C/\Delta C}$ retina, I performed immunofluorescent analyses of retinal sections using antibodies against Rhodopsin (a marker for rod outer segments), S-opsin (a marker for S-cone outer segments), and M-opsin (a marker for M-cone outer segments). Disorganized rod and cone outer segments, and mislocalization of Rhodopsin, S-opsin, and M-opsin in the ONL were observed in the *Sdccag8*$^{\Delta C/\Delta C}$ retina at P14. (Fig. 10F). I also observed the mislocalization of Rhodopsin in the ONL of the retina injected with adeno-associated virus (AAV)-Sdccag8-shRNA3 (Fig. 10G). To analyze the subcellular localization of Sdccag8, I immunostained Sdccag8 and γ-tubulin in the photoreceptors of the *Sdccag8*$^{\Delta C/\Delta C}$ retina and found that Sdccag8 signals at basal bodies in *Sdccag8*$^{\Delta C/\Delta C}$ photoreceptors were lower than those in *Sdccag8*$^{+/+}$ photoreceptors (Figs. 11A and B), suggesting the weak localization of Sdccag8 at basal bodies in *Sdccag8*$^{\Delta C/\Delta C}$ photoreceptors. Next, I immunostained acetylated α-tubulin and observed that the number of photoreceptor cilia significantly decreased in the *Sdccag8*$^{\Delta C/\Delta C}$ retina compared with that in the *Sdccag8*$^{+/+}$ retina (Figs. 11C and D). Unexpectedly, I found that the number of elongated photoreceptor cilia significantly increased in the *Sdccag8*$^{\Delta C/\Delta C}$ retina compared with that in the *Sdccag8*$^{+/+}$ retina (Figs. 11E and F). On the other hand, I immunostained IFT88 in photoreceptor cilia of the *Sdccag8*$^{\Delta C/\Delta C}$ retina and observed no significant difference in the ciliary localization of IFT88 between *Sdccag8*$^{+/+}$ and *Sdccag8*$^{\Delta C/\Delta C}$ photoreceptors (Fig. 11G and H). Taken together, these results suggest that Sdccag8-C is essential for photoreceptor cilia formation.

To investigate whether the loss of Sdccag8-C affects photoreceptor function, we measured the electroretinograms (ERGs) of *Sdccag8*$^{\Delta C/\Delta C}$ mice under dark-adapted (scotopic) and light-adapted (photopic) conditions. We observed that the amplitudes of a-waves (photoreceptors) and b-waves (ON bipolar cells) of *Sdccag8*$^{\Delta C/\Delta C}$ mice under both scotopic and photopic conditions significantly decreased compared with those of *Sdccag8*$^{+/+}$ mice at 6 wks (Figs. 12A-F). These results indicate that rod and cone photoreceptor function is impaired by the Sdccag8-C deficiency.

Deficiency of the C-terminal region of Sdccag8 causes renal degeneration

To investigate the role of Sdccag8-C in the kidney, I first observed the gross appearance of the *Sdccag8*$^{\Delta C/\Delta C}$ kidney. Anemic kidneys were observed in *Sdccag8*$^{\Delta C/\Delta C}$ mice at 3M (Fig. 13A). Next, I performed hematoxylin and eosin (H&E) staining using renal sections from *Sdccag8*$^{+/+}$ and *Sdccag8*$^{\Delta C/\Delta C}$ mice at 6 wks and 3M. The H&E staining showed progressive cyst formation in the *Sdccag8*$^{\Delta C/\Delta C}$ kidney from 6 wks to 3M (Fig. 13B). To examine renal interstitial fibrosis, which are observed in patients with NPHP (Hildebrandt and Zhou, 2007), in the *Sdccag8*$^{\Delta C/\Delta C}$ kidney, I performed Masson trichrome staining using renal sections from *Sdccag8*$^{+/+}$ and *Sdccag8*$^{\Delta C/\Delta C}$ mice at 3M. This revealed interstitial fibrosis in the *Sdccag8*$^{\Delta C/\Delta C}$ kidney (Fig. 13C). These results suggest that *Sdccag8*$^{\Delta C/\Delta C}$ mice exhibit NPHP-like phenotypes, and the loss of Sdccag8-C leads to cyst formation, interstitial fibrosis, and subsequent renal degeneration.

Deficiency of the C-terminal region of Sdccag8 causes impaired spermatogenesis

It has previously been reported that patients with mutations in *SDCCAG8* gene display hypogonadism and hypogenitalism (Schaefer et al., 2011); however, the role of Sdccag8

in the testis remains unclear. I analyzed the testes from *Sdccag8*$^{\Delta C/\Delta C}$ mice and observed that the testes of *Sdccag8*$^{\Delta C/\Delta C}$ mice were smaller than those of *Sdccag8*$^{+/+}$ mice (Fig. 14A). To examine the roles of Sdccag8 in the testes, I performed histological analyses using testicular sections from male *Sdccag8*$^{+/+}$ and *Sdccag8*$^{\Delta C/\Delta C}$ mice. H&E staining showed a lack of mature sperm with long tails in the seminiferous tubules of the *Sdccag8*$^{\Delta C/\Delta C}$ testis at 6 wks, indicating that production of mature sperm is diminished in the *Sdccag8*$^{\Delta C/\Delta C}$ testes (Fig. 14B). In contrast, we observed spermatogonia, spermatocytes, and spermatids in the *Sdccag8*$^{\Delta C/\Delta C}$ testis, suggesting that the mitosis and meiosis phases in the *Sdccag8*$^{\Delta C/\Delta C}$ testis are normal. Furthermore, Leydig and Sertoli cells were also observed in the *Sdccag8*$^{\Delta C/\Delta C}$ testes. Taken together, our results suggest that Sdccag8-C is required for normal spermatogenesis. Sdccag8 may play a role in sperm flagella formation.

Discussion

In the current study, we screened and found that Ick and Mak interact with Sdccag8-C. To analyze the roles of Sdccag8-C *in vivo*, we generated *Sdccag8*$^{\Delta C/\Delta C}$ mice, in which Sdccag8-C was truncated, by the CRISPR-mediated stop codon knock-in strategy. We observed ciliopathy-like organ phenotypes, including cleft palate, polydactyly, retinal and renal degeneration, and abnormal spermatogenesis in *Sdccag8*$^{\Delta C/\Delta C}$ mice, although there may be defects in other tissues. Indeed, we also found ciliary abnormalities in *Sdccag8*$^{\Delta C/\Delta C}$ mice, suggesting that Sdccag8-C is required for normal cilia formation and function. Previous reports showed that *Sdccag8* knockout mice mostly die after birth and that *Sdccag8* gene-trap mice are present at Mendelian ratios at weaning age (Airik et al., 2014; Insolera et al., 2014). Unlike *Sdccag8* knockout mice and *Sdccag8* gene-trap mice, *Sdccag8*$^{\Delta C/\Delta C}$ mice showed partial postnatal lethality. Together, our findings and previous reports suggest that *Sdccag8*$^{\Delta C/\Delta C}$ mice can be used as a distinct and useful mouse model to understand the pathological mechanisms underlying the ciliopathies associated with mutations in *SDCCAG8* gene.

In the *Sdccag8*$^{\Delta C/\Delta C}$ testis, we observed a lack of mature sperm with long tails in seminiferous tubules, suggesting that Sdccag8-C is required for normal spermatogenesis. Since previous studies have shown that *Sdccag8* as well as *Ick* is expressed in spermatocytes and spermatids in the mature testes (Kamio et al., 2010), Sdccag8 may play a role in sperm flagella formation in a cell autonomous manner. However, we cannot exclude the possibility that dysfunction of Leydig cells and/or Sertoli cells by the loss of Sdccag8-C leads to the abnormal spermatogenesis in the *Sdccag8*$^{\Delta C/\Delta C}$ testis. In addition, we have to consider the possible dysfunction of the hypothalamus and/or pituitary gland in *Sdccag8*$^{\Delta C/\Delta C}$ mice. Our findings provide insights into the pathological mechanisms

underlying hypogonadism and hypogenitalism in patients with mutations in *SDCCAG8* gene and the roles of Sdccag8 in the testis. Understanding the detailed molecular and pathological mechanisms of Sdccag8 dysfunction in the testis awaits future analyses.

How is Sdccag8-C involved in cilia formation and function? We found that Sdccag8-C interacts with Ick and Mak proteins by immunoprecipitation assay. We previously found that Ick localizes mainly to the ciliary tips; however, several studies have reported that Ick also localizes to the ciliary base (Broekhuis et al., 2014; Chaya et al., 2014; Moon et al., 2014). In addition, we previously found that Mak localizes to the connecting cilia and ciliary axonemes, as well as basal bodies in retinal photoreceptor cells (Omori et al., 2010). Given that Sdccag8 localizes to centrosomes and basal bodies (Kenedy et al., 2003; Otto et al., 2010), Sdccag8 is suggested to colocalize with Ick and Mak at basal bodies. We found a decrease in ciliated cell number, cilia length, and *Gli1* expression level in *Sdccag8*$^{\Delta C/\Delta C}$ MEFs. These phenotypes in *Sdccag8*$^{\Delta C/\Delta C}$ MEFs were similarly observed in *Ick*-deficient MEFs (Chaya et al., 2014). Furthermore, retinal photoreceptor cells in *Sdccag8*$^{\Delta C/\Delta C}$ mice showed the mislocalization of Rhodopsin and elongated cilia, which were also observed in the *Mak*-deficient retina (Omori et al., 2010). In contrast, unlike *Ick*- and *Mak*-deficient mice, *Sdccag8*$^{\Delta C/\Delta C}$ mice showed no obvious and significant differences in the ciliary localization of IFT88 and Smo. Ick and Mak have been proposed to serve as regulators of IFT turnaround at the ciliary tip and cilia length in mammals (Omori et al., 2010; Broekhuis et al., 2014; Chaya et al., 2014; Moon et al., 2014; Okamoto et al., 2017; Chaya and Furukawa, 2021). Remarkably, *Caenorhabditis elegans* DYF-5, an ortholog of Ick and Mak, was proposed to regulate cilia length and morphology via modulation of microtubule stability rather than IFT (Maurya et al., 2019). Ick and Mak may modulate cilia length independent of IFT regulation, through interaction

with Sdccag8 at the ciliary base. In humans, mutations in *ICK* and *MAK* genes have been reported to lead to retinal degeneration, cystic kidneys, genital abnormalities, and respiratory failure (Lahiry et al., 2009; Ozgul et al., 2011; Tucker et al., 2011; Oud et al., 2016; Paige Taylor et al., 2016), which are also associated with human *SDCCAG8* mutations (Otto et al., 2010; Schaefer et al., 2011; Billingsley et al., 2012; Yamamura et al., 2017; Watanabe et al., 2019; Bahmanpour et al., 2021). Furthermore, pathogenic variants in the *ICK* gene have been linked to juvenile myoclonic epilepsy (Bailey et al., 2018). A previous study reported that a patient with a mutation in the *SDCCAG8* gene displayed epilepsy (Yamamura et al., 2017). Collectively, our observations and previous reports suggest that Sdccag8 functionally interacts with Ick and Mak. However, since the yeast two-hybrid screening identified other proteins that interact with the Ick protein, we cannot exclude the possibility that Ick and Mak interact and function with other proteins at basal bodies.

We observed that Sdccag8-FL and -C localize to centrosomes in NIH-3T3 cells, whereas signals of Sdccag8-N, -M, -NM, -C1, -C2, -C3, and -C4 could not be detected at centrosomes, suggesting that Sdccag8-C serves as a module localizing at basal bodies. We also observed weak localization of Sdccag8 to centrosomes and/or basal bodies in *Sdccag8*$^{\Delta C/\Delta C}$ MEFs and photoreceptor cells. How does Sdccag8-C play key roles in the localization of Sdccag8 to basal bodies? Sdccag8-C consists of coiled-coil motifs that are commonly associated with protein-protein interactions (Burkhard et al., 2001; Otto et al., 2010). Several centrosomal/basal body proteins recruit interacting partners to the basal bodies (Joo et al., 2013; Tanos et al., 2013; Ye et al., 2014). It is possible that Sdccag8 localizes to basal bodies via the interaction of Sdccag8-C with centrosomal/basal body proteins including Ick and Mak. For example, previous studies reported that SDCCAG8-

C interacts with oral-facial-digital syndrome 1 (OFD1), a centrosomal/basal body protein associated with OFD, Joubert syndrome, and retinitis pigmentosa (Ferrante et al., 2001; Coene et al., 2009; Otto et al., 2010; Webb et al., 2012). Furthermore, it was previously reported that SDCCAG8-C interacts with RAB GTPase binding effector protein 2 (RABEP2) that localizes to basal bodies and is required for cilia formation (Airik et al., 2016). Given that Sdccag8 also interacts with Ick and Mak, Sdccag8 may play a key role as the hub of the ciliary/basal body protein-protein interaction network.

In human *SDCCAG8* gene, mutations that are predicted to truncate the Sdccag8 C-terminus were reported to be associated with multiple organ defects, including retinal degeneration and cystic kidney (Otto et al., 2010; Schaefer et al., 2011; Billingsley et al., 2012). Our results suggest that Sdccag8-C is an Ick and Mak-interacting module that is required for the localization of Sdccag8 to centrosomes/basal bodies. In addition, Sdccag8-C is essential for cilia formation and thereby organ development and homeostasis. The current findings shed light on the pathological mechanisms underlying the ciliopathies associated with mutations in *SDCCAG8* gene. Additional mechanistic studies focusing on the relationship between Sdccag8 and the serine-threonine kinases Ick and Mak will advance our understanding of the detailed molecular and pathological mechanisms underlying the ciliopathies.

Material and Methods

Animal care

All procedures conformed to the ARVO Statement for the Use of Animals in Ophthalmic and Vision Research, and these procedures were approved by the Institutional Safety Committee on Recombinant DNA Experiments (approval ID 04220) and the Animal Experimental Committees of Institute for Protein Research (approval ID 29-01-4), Osaka University, and were performed in compliance with the institutional guidelines. Mice were housed in a temperature-controlled room at 22 °C with a 12 h light/dark cycle. Fresh water and rodent diet were available at all times.

Phylogenic analysis

A phylogenic tree of ICK was generated by the neighbor-joining method using MEGA 7. The following accession numbers were used: NP_055735.1 (*Homo sapiens*), XP_014992015.1 (*Macaca mulatta*), NP_001157252.1 (*Mus musculus*), XP_419912.3 (*Gallus gallus*), XP_002934912.2 (*Xenopus tropicalis*), XP_020565302.1 (*Oryzias latipes*), NP_723501.2 (*Drosophila melanogaster*), NP_001129786.2 (*Caenorhabditis elegans*), and AAO86687.1 (*Chlamydomonas reinhardtii*).

Generation of *Sdccag8* Arg537Stop knock-in (*Sdccag8*$^{\Delta C/\Delta C}$) mice

Sdccag8$^{\Delta C/\Delta C}$ mice were generated using the Alt-R® CRISPR-Cas9 system (IDT). The crRNA (IDT) was designed to target exon 13 of the *Sdccag8* gene using CRISPRdirect (http://crispr.dbcls.jp/). Single-stranded DNA (ssDNA) (IDT) containing an Arg537Stop codon and an EcoRI restriction site was also designed with 60 bp homology sequences

on each side of the targeting codon. The crRNA and tracrRNA (IDT) in a duplex buffer (IDT) were incubated at 37 °C for 5 min and returned to room temperature. The guide RNA complex was mixed with Cas9 nuclease 3NLS (IDT), incubated at room temperature for 5 min, and then mixed with ssDNA in Opti-MEM (Gibco) before electroporation. The ribonucleoprotein complex and ssDNA were electroporated into the fertilized one-cell eggs of B6C3F1 mice. The founder mouse was then backcrossed with the C57BL/6J mice.

Plasmid construction

Plasmids expressing FLAG or HA-tagged Ick, FLAG-tagged EGFP and EGFP were previously constructed (Omori et al., 2010; Chaya et al., 2014). Full-length cDNA fragments of mouse *Mak* and *Sdccag8* were amplified by PCR using mouse retinal cDNA as a template and subcloned into the pCAGGSII-3xFLAG and pCAGGSII-2xHA vectors (Irie et al., 2015). The cDNA fragments encoding the mouse Sdccag8-N, Sdccag8-M and Sdccag8-C were amplified by PCR using mouse retinal cDNA as a template and subcloned into the pCAGGSII-3xFLAG vector. The cDNA fragment encoding the mouse Sdccag8-NM, Sdccag8-C1, Sdccag8-C2, Sdccag8-C3, and Sdccag8-C4 were amplified by PCR using the plasmid encoding full-length Sdccag8 as a template and subcloned into the pCAGGSII-3xFLAG vector. A full-length cDNA fragment of human *SDCCAG8* was amplified by PCR using human retinal cDNA (Clontech) as a template and subcloned into the pCAGGSII-3xFLAG vector. The cDNA fragment encoding the human SDCCAG8-NM was amplified by PCR using the plasmid encoding full-length human SDCCAG8 as a template and subcloned into the pCAGGSII-3xFLAG vector. The cDNA fragment encoding EGFP was amplified by PCR using the plasmid encoding EGFP as a template

and subcloned into the pCAGGSII-2xHA vector. For *Sdccag8* knockdown, the Sdccag8-shRNA and shRNA-control cassette was subcloned into pBAsi-mU6 vector (Takara). The target sequences were as follows: Sdccag8-shRNA1, 5'-GCACAGCCATGCTGTC AATCA-3'; Sdccag8-shRNA2, 5'-GGAGACATTGAGGGAGCAAAC-3'; Sdccag8-shRNA3, 5'-GCGCAGAAGAGAGAGACAAGT-3'; shRNA-control, 5'-GACGTCTAA CGGATTCGAGCT-3' (Itoh et al., 2013). For the production of AAV-Sdccag8-shRNA and AAV-shRNA-control, the mU6-Sdccag8-shRNA3 or mU6-shRNA-control fragment was inserted into the pAAV-CAG-AcGFP vector (Kozuka et al., 2019). Primer sequences used for amplification are shown in Table 2.

Yeast two-hybrid screening

Yeast two-hybrid screening was performed as described previously (Ueno et al., 2018). In brief, we performed a yeast two-hybrid screen using the MATCHMAKER GAL4 Two-Hybrid System3 (Takara Bio). The open reading frame of mouse Ick was inserted into the pGBKT7 bait plasmid and transformed into the AH109 yeast strain. We screened 1.0×10^6 transformants from a one-to-one mixture of mouse E17 whole embryos and the P0-P3 retinal cDNA library. Positive colonies were identified on the basis of their ability to express the nutritional markers ADE2 and HIS3 by plating on synthetic defined (SD) (-Trp, -Leu, -Ade, -His) medium. The plasmids were isolated from yeast using Zymoprep Yeast Plasmid Miniprep I (Zymo Research) and transformed into E. coli DH5α.

Cell culture and transfection

Sdccag8$^{+/+}$ and *Sdccag8*$^{\Delta C/\Delta C}$ MEFs were derived from embryonic day 13.5 embryos and cultured in DMEM (Sigma) containing 10% fetal bovine serum supplemented with

penicillin (100 μg/ml) and streptomycin (100 μg/ml) at 37 °C with 5% CO_2. To induce ciliogenesis in MEFs, cells were grown to 80-90 % confluency and serum-starved for 24 h. HEK293T and NIH-3T3 cells were cultured in DMEM containing 10% fetal bovine and calf serum, respectively, supplemented with penicillin (100 μg/ml) and streptomycin (100 μg/ml) at 37 °C with 5% CO_2. Transfection was performed with the calcium phosphate method for HEK293T cells or Lipofectamine LTX (Invitrogen) for NIH-3T3 cells. To induce ciliogenesis in transfected cells, the medium was replaced by serum-free medium at 24 or 48 h after the transfection, and cells were cultured for 24 h in serum-free medium.

Immunoprecipitation assay

Immunoprecipitation assays were performed as previously described (Chaya et al., 2019). HEK293T cells were co-transfected with plasmids expressing FLAG and HA-tagged proteins. After 48 h of transfection, the cells were lysed in a lysis buffer supplemented with protease inhibitors (20 mM tris (hydroxymethyl) aminomethane (Tris)-HCl pH 7.5, 150 mM NaCl, 1% Nonidet P-40 (NP-40), 1 mM ethylenediaminetetraacetate (EDTA), 1 mM phenylmethylsulfonyl fluoride (PMSF), 2 μg/ml leupeptin, 5 μg/ml aprotinin, and 3 μg/ml pepstatin A). The cell lysates were centrifuged twice at 15,100 g for 5 min. The supernatants were incubated with an anti-FLAG M2 affinity gel (Sigma-Aldrich) overnight at 4 °C. The beads were washed five times with wash buffer (20 mM Tris-HCl pH 7.5, 150 mM NaCl, 1% NP-40, and 1 mM EDTA) and then eluted with elution buffer (20 mM Tris-HCl pH 7.5, 150 mM NaCl, 5 mg/ml 1 × FLAG peptide) for 30 min at 4 °C. The immunoprecipitated samples were incubated with sodium dodecyl sulfate (SDS)-sample buffer for 30 min at room temperature and analyzed by Western blot. For

immunoprecipitation from HEK293T cell lysates, the cells were lysed in a RIPA buffer supplemented with protease inhibitors and phosphatase inhibitor cocktail (Roche) (20 mM Tris-HCl pH 7.5, 150 mM NaCl, 1% NP-40, 1 mM EDTA, 0.5% sodium deoxycholate, 0.1% SDS, 1 mM PMSF, 2 μg/ml leupeptin, 5 μg/ml aprotinin, and 3 μg/ml pepstatin A). The cell lysates and antibodies were incubated overnight at 4 °C, and then were incubated for 6 h at 4 °C with Protein A Sepharose 4 Fast Flow (GE Healthcare). The beads were washed five times with wash buffer (20 mM Tris-HCl pH 7.5, 150 mM NaCl, 1% NP-40, 1 mM EDTA, 0.5% sodium deoxycholate, 0.1% SDS). The immunoprecipitated samples were incubated with SDS-sample buffer for 5 min at 100 °C and analyzed by Western blot.

Western blot analysis

Western blot analysis was performed as described previously (Omori et al., 2017). Briefly, HEK293T cells were lysed in a lysis buffer supplemented with protease inhibitors (20 mM Tris-HCl pH 7.5, 150 mM NaCl, 1% NP-40, 1 mM EDTA, 1 mM PMSF, 2 μg/ml leupeptin, 5 μg/ml aprotinin, and 3 μg/ml pepstatin A) or RIPA buffer supplemented with protease inhibitors and phosphatase inhibitor cocktail (Roche) (20 mM Tris-HCl pH 7.5, 150 mM NaCl, 1% NP-40, 1 mM EDTA, 0.5% sodium deoxycholate, 0.1% SDS, 1 mM PMSF, 2 μg/ml leupeptin, 5 μg/ml aprotinin, and 3 μg/ml pepstatin A). The samples were resolved by SDS-polyacrylamide gel electrophoresis (PAGE) and transferred to PVDF membrane using semidry transfer cells (Bio-Rad or iBlot system; Invitrogen). The membranes were blocked with blocking buffer (3% skim milk, and 0.05% Tween 20 in Tris-buffered saline). Signals were detected using Chemi-Lumi One L (Nakalai Tesque) or Pierce Western Blotting Substrate Plus (Thermo Fisher Scientific). We used the

following primary antibodies: rabbit anti-FLAG (1:5,000, Sigma, F7425); rat anti-HA (1:2,500 or 1:5,000, Roche, 3F10); rabbit anti-GFP (1:5,000, MBL, 598); guinea pig anti-Ick (1:50) (Chaya et al., 2014); rabbit anti-Sdccag8 (1:200, Proteintech, 13471-1-AP). The following secondary antibodies were used: horseradish peroxidase-conjugated anti-rabbit IgG (1:10,000, Jackson Laboratory), anti-rat IgG (1:10,000, Jackson Laboratory), and anti-guinea pig IgG (1:10,000, Jackson Laboratory).

Immunofluorescent analysis of cells and retinal sections

Immunofluorescent analysis of cells and retinal sections was performed as described previously (Omori et al., 2010). Cells were washed with phosphate-buffered saline (PBS), fixed with 4% paraformaldehyde (PFA) in PBS for 5 min at room temperature or cold methanol for 5 min at -20 °C, and subsequently incubated with blocking buffer (5% normal donkey serum, and 0.1% Triton X-100 in PBS) for 30 min at room temperature, and then immunostained with primary antibodies in the blocking buffer overnight at 4 °C. Cells were washed with PBS and incubated with secondary antibodies and DAPI (1:1000, Nacalai Tesque) in the blocking buffer for 2-4 h at room temperature. Mouse eyes were fixed in 4% PFA in PBS for 15 sec, 5 min or 10 min at room temperature, embedded in TissueTec OCT compound 4583 (Sakura), frozen, and cryosectioned at 20 μm thickness. Frozen sections on slides were dried overnight at room temperature, rehydrated in PBS, incubated with the blocking buffer, and then immunostained with primary antibodies in the blocking buffer overnight at 4 °C. Slides were washed with PBS and incubated with secondary antibodies and DAPI in the blocking buffer for 2-4 h at room temperature. The specimens were observed under a laser confocal microscope (LSM700 or LSM710, Carl Zeiss). We used the following primary antibodies: rabbit anti-FLAG (1:5,000, Sigma,

F7425); rat anti-HA (1: 1000, Roche, 3F10); mouse anti-acetylated α tubulin (1:1,000 or 1:2,000, Sigma, 6-11B-1); rabbit anti-IFT88 (1:1,000, Proteintech, 13967-1-AP); rabbit anti-Arl13b (1:500, Proteintech, 17711-1-AP); mouse anti-Smo (1:150, Santa Cruz, sc-166685); rabbit anti-Rhodopsin (1:2,500, LSL, LB-5597), goat anti-S-opsin (1:500, Santa Cruz, sc-14363); rabbit anti-M-opsin (1:300, Millipore, AB5405); rabbit anti-Sdccag8 (1:250 or 1:500, Proteintech, 13471-1-AP); rat anti-GFP (1:1,000, Nacalai Tesque, 04404-84); mouse anti-γ-tubulin (1:300, Sigma, T6557); rabbit IgG isotype control (same concentration as anti-Sdccag8 (1:500, Proteintech, 13471-1-AP), Abcam, ab172730). Cy3-conjugated (1:500, Jackson ImmunoResearch Laboratories), DyLight 649-conjugated (1:500, Jackson ImmunoResearch Laboratories) or Alexa Fluor 488-conjugated (1:500, Sigma) secondary antibodies were used.

RT-PCR and qRT-PCR analyses

RT-PCR and qRT-PCR analyses were performed as described previously (Tsutsumi et al., 2018; Sugiyama et al., 2020). Total RNAs were isolated from MEFs and mouse tissues, including the retina, cerebrum, cerebellum, brain stem, thymus, heart, lung, kidney, liver, spleen, muscle, intestine, ovary, and testis, using TRIzol RNA extraction reagent (Invitrogen). The total RNA (0.5 or 2 μg) was reverse transcribed into cDNA using PrimeScript RT reagent or PrimeScript II reagent (Takara). The cDNAs were used as templates for RT-PCR reactions with rTaq polymerase (Takara). qRT-PCR was performed using a SYBR GreenER qPCR Super Mix Universal (Invitrogen) and Thermal Cycler Dice Real Time System Single MRQ TP700 (Takara) according to the manufacturer's instructions. Quantification was performed by Thermal Cycler Dice Real Time System software version 2.11 (Takara). Primer sequences used for amplification are shown in

Table 2.

In situ hybridization

Retinal tissues from P14 mice and brain tissues from 4 wks mice were dissected and freshly frozen. Testicular tissues from 16 wks mice and intestinal tissues from 8 wks mice were dissected and fixed in 4% PFA in PBS overnight at 4 °C or room temperature. The tissues were then equilibrated in 30% sucrose in PBS overnight at 4 °C, embedded in TissueTec OCT compound 4583 (Sakura, Japan), frozen, and cryosectioned at 8, 14 or 30 μm. Generation of a digoxigenin-labeled riboprobe and *in situ* hybridization were performed as described previously (Irie et al., 2015). Primer sequences used for amplification of the cDNA fragments of *Lgr5*, *Slc5a1*, and *Wnt3* are shown in Table 2. Primer sequences used for amplification of the cDNA fragments of *Ick*, *Acr*, *Clgn*, *PLZF*, *Sox9*, and *3β-HSD* were as described previously (Chaya et al., 2014; Mizuhashi et al., 2015). The cDNA fragment encoding the Sdccag8-NM was used to synthesize the riboprobe.

Toluidine blue staining

Toluidine blue staining of retinal sections was performed as described previously (Chaya et al., 2017). Retinal sections were rinsed with PBS and stained with 0.1% toluidine blue in PBS for 30 sec. After washing with PBS, slides were coverslipped and immediately observed under the microscope. ONL and INL+IPL+GCL thicknesses were measured and quantified with National Institutes of Health ImageJ software.

AAV production and subretinal injection

AAV production and subretinal injection of AAVs were performed as previously described (Watanabe et al., 2013). AAVs were produced by triple transfection of an AAV vector plasmid, an adenovirus helper plasmid, and an AAV helper plasmid (pXR5) into AAV-293 cells using the calcium phosphate method. The cells were harvested 72 h after transfection and lysed in four freeze-thaw cycles. The supernatant was collected by centrifugation and treated with benzonase nuclease (Novagen). The viruses were purified using an iodixanol gradient. The gradient was formed in Ultra-Clear centrifuge tubes (14×95 mm, Beckman) by first adding 54% iodixanol (Axis-Shield) in PBS-MK buffer (1×PBS, 1 mM $MgCl_2$, and 25 mM KCl), followed by overlaying 40% iodixanol in PBS-MK buffer, 25% iodixanol in PBS-MK buffer containing phenol red, and 15% iodixanol in PBS-MK buffer containing 1 M NaCl. The tubes were centrifuged at 40,000 rpm in an SW40Ti rotor. The 54%-40% fraction containing virus was collected using an 18-gauge needle and concentrated using an Amicon Ultra Centrifugal Filter Ultracel-100K (Millipore). The titer of each AAV (in vector genomes (VG)/ml) was determined by qPCR using SYBR GreenER Q-PCR Super Mix (Invitrogen) and Thermal Cycler Dice Real Time System Single MRQ TP700 (Takara). The primers used for the AAV titrations are listed in Table 2. The titers of AAV-shRNA-control and AAV-Sdccag8-shRNA3 were adjusted to approximately 2×10^{12} VG/ml. 0.3 μl of the AAV preparations was injected into the subretinal spaces of the P0 ICR mice. The injected retinas were harvested at P15.

ERG analysis

ERG analysis was performed as described previously (Kubo et al., 2021). Briefly, ERG responses were measured by the PuREC system with LED LS-100 (Mayo). Mice were dark-adapted overnight, and then anesthetized with an intraperitoneal injection of 100

mg/kg ketamine and 10 mg/kg xylazine diluted in saline (Otsuka). The mice were placed on a heating pad and stimulated with four stroboscopic stimuli ranging from −4.0 to 1.0 log cd s/m^2 for scotopic ERGs. After the mice were light-adapted for 10 min, they were stimulated with four stroboscopic stimuli ranging from −0.5 to 1.0 log cd s/m^2 for photopic ERGs. The photopic ERGs were recorded on a rod-suppressing white background of 1.3 log cd s/m^2.

H&E staining and Masson trichrome staining

H&E and Masson trichrome stainings were commissioned to Applied Medical Research Laboratory (Osaka, Japan). Mouse kidneys and testes were fixed with 4% PFA in PBS for 72 h at 4 °C and bouin solution for 20 h at 4 °C, respectively, embedded in paraffin, and sectioned at 5 μm thickness.

Statistical analysis

Data are presented as mean ± SD. Statistical significance was evaluated using unpaired *t*-test, one-way ANOVA, or two-way ANOVA. A value of $p < 0.05$ was taken to be statistically significant.

References

Airik R, Schueler M, Airik M, Cho J, Ulanowicz KA, Porath JD, Hurd TW, Bekker-Jensen S, Schroder JM, Andersen JS, Hildebrandt F (2016) SDCCAG8 Interacts with RAB Effector Proteins RABEP2 and ERC1 and Is Required for Hedgehog Signaling. PLoS One 11:e0156081.

Airik R, Slaats GG, Guo Z, Weiss AC, Khan N, Ghosh A, Hurd TW, Bekker-Jensen S, Schroder JM, Elledge SJ, Andersen JS, Kispert A, Castelli M, Boletta A, Giles RH, Hildebrandt F (2014) Renal-retinal ciliopathy gene Sdccag8 regulates DNA damage response signaling. J Am Soc Nephrol 25:2573-2583.

Bahmanpour Z, Daneshmandpour Y, Kazeminasab S, Khalil Khalili S, Alehabib E, Chapi M, Soosanabadi M, Darvish H, Emamalizadeh B (2021) A novel splice site mutation in the SDCCAG8 gene in an Iranian family with Bardet-Biedl syndrome. Int Ophthalmol 41:389-397.

Bailey JN et al. (2018) Variant Intestinal-Cell Kinase in Juvenile Myoclonic Epilepsy. N Engl J Med 378:1018-1028.

Billingsley G, Vincent A, Deveault C, Heon E (2012) Mutational analysis of SDCCAG8 in Bardet-Biedl syndrome patients with renal involvement and absent polydactyly. Ophthalmic Genet 33:150-154.

Broekhuis JR, Verhey KJ, Jansen G (2014) Regulation of cilium length and intraflagellar transport by the RCK-kinases ICK and MOK in renal epithelial cells. PLoS One 9:e108470.

Burkhard P, Stetefeld J, Strelkov SV (2001) Coiled coils: a highly versatile protein folding motif. Trends Cell Biol 11:82-88.

Chaya T, Furukawa T (2021) Post-translational modification enzymes as key regulators of ciliary protein trafficking. J Biochem.

Chaya T, Omori Y, Kuwahara R, Furukawa T (2014) ICK is essential for cell type-specific ciliogenesis and the regulation of ciliary transport. EMBO J 33:1227-1242.

Chaya T, Tsutsumi R, Varner LR, Maeda Y, Yoshida S, Furukawa T (2019) Cul3-Klhl18 ubiquitin ligase modulates rod transducin translocation during light-dark adaptation. EMBO J 38:e101409.

Chaya T, Matsumoto A, Sugita Y, Watanabe S, Kuwahara R, Tachibana M, Furukawa T (2017) Versatile functional roles of horizontal cells in the retinal circuit. Sci Rep 7:5540.

Chen JK, Taipale J, Young KE, Maiti T, Beachy PA (2002) Small molecule modulation of Smoothened activity. Proc Natl Acad Sci U S A 99:14071-14076.

Cheng CY, Mruk DD (2002) Cell junction dynamics in the testis: Sertoli-germ cell interactions and male contraceptive development. Physiol Rev 82:825-874.

Coene KL, Roepman R, Doherty D, Afroze B, Kroes HY, Letteboer SJ, Ngu LH, Budny B, van Wijk E, Gorden NT, Azhimi M, Thauvin-Robinet C, Veltman JA, Boink M, Kleefstra T, Cremers FP, van Bokhoven H, de Brouwer AP (2009) OFD1 is mutated in X-linked Joubert syndrome and interacts with LCA5-encoded lebercilin. Am J Hum Genet 85:465-481.

Ferrante MI, Giorgio G, Feather SA, Bulfone A, Wright V, Ghiani M, Selicorni A, Gammaro L, Scolari F, Woolf AS, Sylvie O, Bernard L, Malcolm S, Winter R, Ballabio A, Franco B (2001) Identification of the gene for oral-facial-digital type I syndrome. Am J Hum Genet 68:569-576.

Flynn M, Whitton L, Donohoe G, Morrison CG, Morris DW (2020) Altered gene regulation as a candidate mechanism by which ciliopathy gene SDCCAG8 contributes to schizophrenia and cognitive function. Hum Mol Genet 29:407-417.

Fuentealba LC, Rompani SB, Parraguez JI, Obernier K, Romero R, Cepko CL, Alvarez-Buylla A (2015) Embryonic Origin of Postnatal Neural Stem Cells. Cell 161:1644-1655.

Gerbe F, Sidot E, Smyth DJ, Ohmoto M, Matsumoto I, Dardalhon V, Cesses P, Garnier L, Pouzolles M, Brulin B, Bruschi M, Harcus Y, Zimmermann VS, Taylor N, Maizels RM, Jay P (2016) Intestinal epithelial tuft cells initiate type 2 mucosal immunity to helminth parasites. Nature 529:226-230.

Gerdes JM, Davis EE, Katsanis N (2009) The vertebrate primary cilium in development, homeostasis, and disease. Cell 137:32-45.

Hildebrandt F, Zhou W (2007) Nephronophthisis-associated ciliopathies. J Am Soc Nephrol 18:1855-1871.

Hildebrandt F, Benzing T, Katsanis N (2011) Ciliopathies. N Engl J Med 364:1533-1543.

Huangfu D, Anderson KV (2005) Cilia and Hedgehog responsiveness in the mouse. Proc Natl Acad Sci U S A 102:11325-11330.

Insolera R, Shao W, Airik R, Hildebrandt F, Shi SH (2014) SDCCAG8 regulates pericentriolar material recruitment and neuronal migration in the developing cortex. Neuron 83:805-822.

Irie S, Sanuki R, Muranishi Y, Kato K, Chaya T, Furukawa T (2015) Rax Homeoprotein Regulates Photoreceptor Cell Maturation and Survival in Association with Crx in the Postnatal Mouse Retina. Mol Cell Biol 35:2583-2596.

Ishikawa H, Marshall WF (2011) Ciliogenesis: building the cell's antenna. Nat Rev Mol Cell Biol 12:222-234.

Itoh Y, Moriyama Y, Hasegawa T, Endo TA, Toyoda T, Gotoh Y (2013) Scratch regulates neuronal migration onset via an epithelial-mesenchymal transition-like mechanism. Nat Neurosci 16:416-425.

Joo K, Kim CG, Lee MS, Moon HY, Lee SH, Kim MJ, Kweon HS, Park WY, Kim CH, Gleeson JG, Kim J (2013) CCDC41 is required for ciliary vesicle docking to the mother centriole. Proc Natl Acad Sci U S A 110:5987-5992.

Kamio T, Asano A, Hosaka YZ, Khalid AM, Yokota S, Ohta M, Ohyama K, Yamano Y (2010) Expression of the centrosomal colon cancer autoantigen gene during spermatogenesis in the maturing rat testis. Biosci Biotechnol Biochem 74:1466-1469.

Kenedy AA, Cohen KJ, Loveys DA, Kato GJ, Dang CV (2003) Identification and characterization of the novel centrosome-associated protein CCCAP. Gene 303:35-46.

Kozuka T, Omori Y, Watanabe S, Tarusawa E, Yamamoto H, Chaya T, Furuhashi M, Morita M, Sato T, Hirose S, Ohkawa Y, Yoshimura Y, Hikida T, Furukawa T (2019) miR-124 dosage regulates prefrontal cortex function by dopaminergic modulation. Sci Rep 9:3445.

Kubo S, Yamamoto H, Kajimura N, Omori Y, Maeda Y, Chaya T, Furukawa T (2021) Functional analysis of Samd11, a retinal photoreceptor PRC1 component, in establishing rod photoreceptor identity. Sci Rep 11:4180.

Lahiry P, Wang J, Robinson JF, Turowec JP, Litchfield DW, Lanktree MB, Gloor GB, Puffenberger EG, Strauss KA, Martens MB, Ramsay DA, Rupar CA, Siu V, Hegele RA (2009) A multiplex human syndrome implicates a key role for intestinal cell kinase in development of central nervous, skeletal, and endocrine systems. Am J Hum Genet 84:134-147.

Lois C, Alvarez-Buylla A (1994) Long-distance neuronal migration in the adult mammalian brain. Science 264:1145-1148.

Lovera M, Luders J (2021) The ciliary impact of nonciliary gene mutations. Trends Cell Biol.

Luo F, Tao YH (2018) Nephronophthisis: A review of genotype-phenotype correlation. Nephrology (Carlton) 23:904-911.

Malicki JJ, Johnson CA (2017) The Cilium: Cellular Antenna and Central Processing Unit. Trends Cell Biol 27:126-140.

Maurya AK, Rogers T, Sengupta P (2019) A CCRK and a MAK Kinase Modulate Cilia Branching and Length via Regulation of Axonemal Microtubule Dynamics in Caenorhabditis elegans. Curr Biol 29:1286-1300 e1284.

McConnachie DJ, Stow JL, Mallett AJ (2021) Ciliopathies and the Kidney: A Review. Am J Kidney Dis 77:410-419.

Ming GL, Song H (2011) Adult neurogenesis in the mammalian brain: significant answers and significant questions. Neuron 70:687-702.

Miyata Y, Nishida E (1999) Distantly related cousins of MAP kinase: biochemical properties and possible physiological functions. Biochem Biophys Res Commun 266:291-295.

Mizuhashi K, Chaya T, Kanamoto T, Omori Y, Furukawa T (2015) Obif, a Transmembrane Protein, Is Required for Bone Mineralization and Spermatogenesis in Mice. PLoS One 10:e0133704.

Moon H, Song J, Shin JO, Lee H, Kim HK, Eggenschwiller JT, Bok J, Ko HW (2014) Intestinal cell kinase, a protein associated with endocrine-cerebro-osteodysplasia syndrome, is a key regulator of cilia length and Hedgehog signaling. Proc Natl Acad Sci U S A 111:8541-8546.

Nigg EA, Raff JW (2009) Centrioles, centrosomes, and cilia in health and disease. Cell 139:663-678.

Okamoto S, Chaya T, Omori Y, Kuwahara R, Kubo S, Sakaguchi H, Furukawa T (2017) Ick Ciliary Kinase Is Essential for Planar Cell Polarity Formation in Inner Ear Hair Cells and Hearing Function. J Neurosci 37:2073-2085.

Omori Y, Chaya T, Katoh K, Kajimura N, Sato S, Muraoka K, Ueno S, Koyasu T, Kondo M, Furukawa T (2010) Negative regulation of ciliary length by ciliary male germ cell-associated kinase (Mak) is required for retinal photoreceptor survival. Proc Natl Acad Sci U S A 107:22671-22676.

Omori Y, Kubo S, Kon T, Furuhashi M, Narita H, Kominami T, Ueno A, Tsutsumi R, Chaya T, Yamamoto H, Suetake I, Ueno S, Koseki H, Nakagawa A, Furukawa T (2017) Samd7 is a cell type-specific PRC1 component essential for establishing retinal rod photoreceptor identity. Proc Natl Acad Sci U S A 114:E8264-E8273.

Otto EA et al. (2010) Candidate exome capture identifies mutation of SDCCAG8 as the cause of a retinal-renal ciliopathy. Nat Genet 42:840-850.

Oud MM et al. (2016) A novel ICK mutation causes ciliary disruption and lethal endocrine-cerebro-osteodysplasia syndrome. Cilia 5:8.

Ozgul RK, Siemiatkowska AM, Yucel D, Myers CA, Collin RW, Zonneveld MN, Beryozkin A, Banin E, Hoyng CB, van den Born LI, European Retinal Disease C, Bose R, Shen W, Sharon D, Cremers FP, Klevering BJ, den Hollander AI, Corbo JC (2011) Exome sequencing and cis-regulatory mapping identify mutations in MAK, a gene encoding a regulator of ciliary length, as a cause of retinitis

pigmentosa. Am J Hum Genet 89:253-264.

Paige Taylor S et al. (2016) An inactivating mutation in intestinal cell kinase, ICK, impairs hedgehog signalling and causes short rib-polydactyly syndrome. Hum Mol Genet 25:3998-4011.

Reiter JF, Leroux MR (2017) Genes and molecular pathways underpinning ciliopathies. Nat Rev Mol Cell Biol 18:533-547.

Rohatgi R, Milenkovic L, Scott MP (2007) Patched1 regulates hedgehog signaling at the primary cilium. Science 317:372-376.

Sato T, van Es JH, Snippert HJ, Stange DE, Vries RG, van den Born M, Barker N, Shroyer NF, van de Wetering M, Clevers H (2011) Paneth cells constitute the niche for Lgr5 stem cells in intestinal crypts. Nature 469:415-418.

Schaefer E et al. (2011) Mutations in SDCCAG8/NPHP10 Cause Bardet-Biedl Syndrome and Are Associated with Penetrant Renal Disease and Absent Polydactyly. Mol Syndromol 1:273-281.

Shinkai Y, Satoh H, Takeda N, Fukuda M, Chiba E, Kato T, Kuramochi T, Araki Y (2002) A testicular germ cell-associated serine-threonine kinase, MAK, is dispensable for sperm formation. Mol Cell Biol 22:3276-3280.

Sugiyama T, Yamamoto H, Kon T, Chaya T, Omori Y, Suzuki Y, Abe K, Watanabe D, Furukawa T (2020) The potential role of Arhgef33 RhoGEF in foveal development in the zebra finch retina. Sci Rep 10:21450.

Tanos BE, Yang HJ, Soni R, Wang WJ, Macaluso FP, Asara JM, Tsou MF (2013) Centriole distal appendages promote membrane docking, leading to cilia initiation. Genes Dev 27:163-168.

Togawa K, Yan YX, Inomoto T, Slaugenhaupt S, Rustgi AK (2000) Intestinal cell kinase (ICK) localizes to the crypt region and requires a dual phosphorylation site found in map kinases. J Cell Physiol 183:129-139.

Tsutsumi R, Chaya T, Furukawa T (2018) Enriched expression of the ciliopathy gene Ick in cell proliferating regions of adult mice. Gene Expr Patterns 29:18-23.

Tucker BA, Scheetz TE, Mullins RF, DeLuca AP, Hoffmann JM, Johnston RM, Jacobson SG, Sheffield VC, Stone EM (2011) Exome sequencing and analysis of induced pluripotent stem cells identify the cilia-related gene male germ cell-associated kinase (MAK) as a cause of retinitis pigmentosa. Proc Natl Acad Sci U S A 108:E569-576.

Ueno A, Omori Y, Sugita Y, Watanabe S, Chaya T, Kozuka T, Kon T, Yoshida S, Matsushita K, Kuwahara R, Kajimura N, Okada Y, Furukawa T (2018) Lrit1, a Retinal Transmembrane Protein, Regulates Selective Synapse Formation in Cone

Photoreceptor Cells and Visual Acuity. Cell Rep 22:3548-3561.

van der Flier LG, van Gijn ME, Hatzis P, Kujala P, Haegebarth A, Stange DE, Begthel H, van den Born M, Guryev V, Oving I, van Es JH, Barker N, Peters PJ, van de Wetering M, Clevers H (2009) Transcription factor achaete scute-like 2 controls intestinal stem cell fate. Cell 136:903-912.

van Praag H, Schinder AF, Christie BR, Toni N, Palmer TD, Gage FH (2002) Functional neurogenesis in the adult hippocampus. Nature 415:1030-1034.

Watanabe S, Sanuki R, Ueno S, Koyasu T, Hasegawa T, Furukawa T (2013) Tropisms of AAV for subretinal delivery to the neonatal mouse retina and its application for in vivo rescue of developmental photoreceptor disorders. PLoS One 8:e54146.

Watanabe Y, Fujinaga S, Sakuraya K, Morisada N, Nozu K, Iijima K (2019) Rapidly Progressive Nephronophthisis in a 2-Year-Old Boy with a Homozygous SDCCAG8 Mutation. Tohoku J Exp Med 249:29-32.

Webb TR, Parfitt DA, Gardner JC, Martinez A, Bevilacqua D, Davidson AE, Zito I, Thiselton DL, Ressa JH, Apergi M, Schwarz N, Kanuga N, Michaelides M, Cheetham ME, Gorin MB, Hardcastle AJ (2012) Deep intronic mutation in OFD1, identified by targeted genomic next-generation sequencing, causes a severe form of X-linked retinitis pigmentosa (RP23). Hum Mol Genet 21:3647-3654.

Yamamura T, Morisada N, Nozu K, Minamikawa S, Ishimori S, Toyoshima D, Ninchoji T, Yasui M, Taniguchi-Ikeda M, Morioka I, Nakanishi K, Nishio H, Iijima K (2017) Rare renal ciliopathies in non-consanguineous families that were identified by targeted resequencing. Clin Exp Nephrol 21:136-142.

Ye X, Zeng H, Ning G, Reiter JF, Liu A (2014) C2cd3 is critical for centriolar distal appendage assembly and ciliary vesicle docking in mammals. Proc Natl Acad Sci U S A 111:2164-2169.

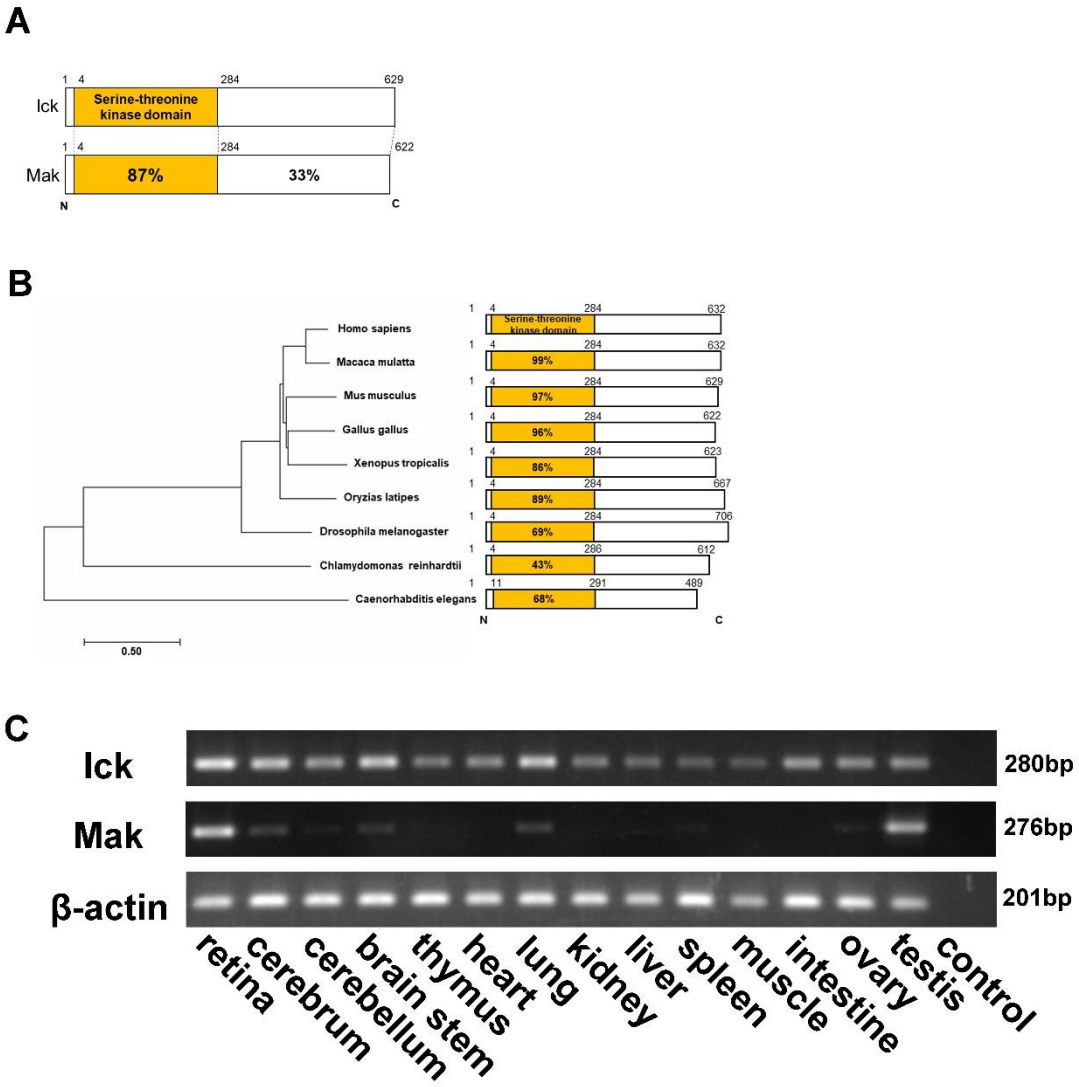

Figure 1. Ick protein conservation and *Ick* expression in adult mouse tissues.

(**A**) Schematic illustration of the amino acid sequence homology between mouse Ick and Mak proteins. Ick and Mak proteins are similar especially in their serine-threonine kinase domains. (**B**) A phylogenic tree and domain structures of ICK orthologs. Each percentage shows the amino acid sequence identity in the serine-threonine kinase domain between human ICK and its orthologs. (**C**) RT-PCR analysis of *Ick, Mak* and *β-actin* in various mouse tissues at 4 wks. *Ick* is ubiquitously expressed in adult tissues.

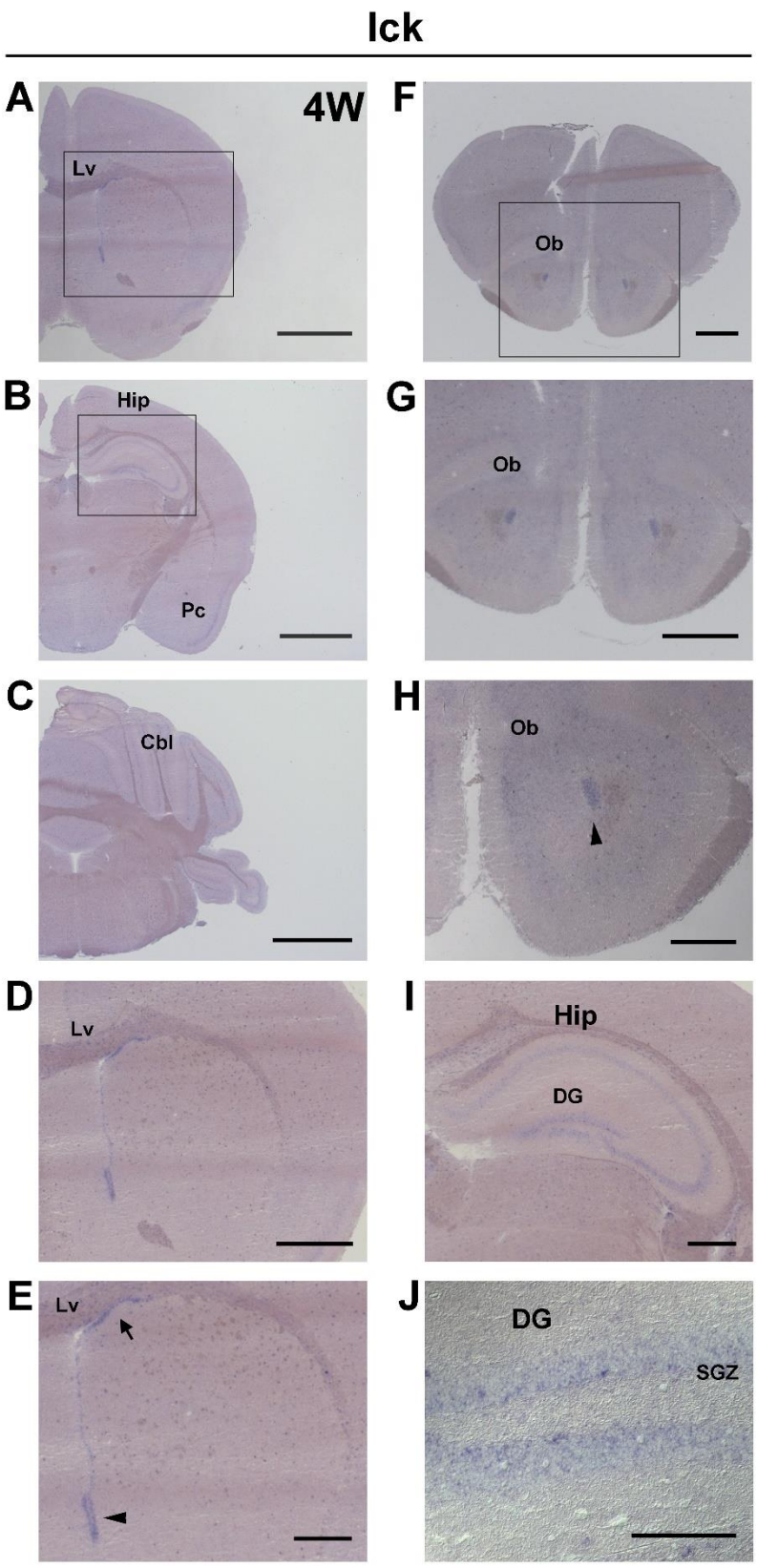

Figure 2. *Ick* expression in the adult brain.

(**A-J**) *In situ* hybridization analysis of mouse *Ick* in coronal brain sections at 4 wks. The *Ick* signal was detected in the lateral ventricle (**A**), hippocampus (**B**), piriform cortex (**B**), cerebellum (**C**), and olfactory bulb (**F**). (**D**) Higher magnification view of the boxed area in (**A**). (**E**) Higher magnification view of (**D**). (**G**) Higher magnification view of the boxed area in (**F**). (**H**) Higher magnification view of (**G**). (**I**) Higher magnification view of the boxed area in (**B**). (**J**) Higher magnification view of the hippocampal DG. The *Ick* signal was detected especially in the dorsal edge (arrow) and ventral tip (arrowhead) of the lateral walls in the lateral ventricle (**E**), RMS in the olfactory bulb (arrowhead) (**H**), and SGZ in the hippocampal DG (**J**). Scale bars, 2 mm (**A-C**), 1 mm (**D**, **F**, **G**), 500 μm (**E**, **H**, **I**), 200 μm (**J**). Lv, lateral ventricle; Hip, hippocampus; Pc, piriform cortex; Cbl, cerebellum; Ob, olfactory bulb; DG, dentate gyrus; SGZ, subgranular zone.

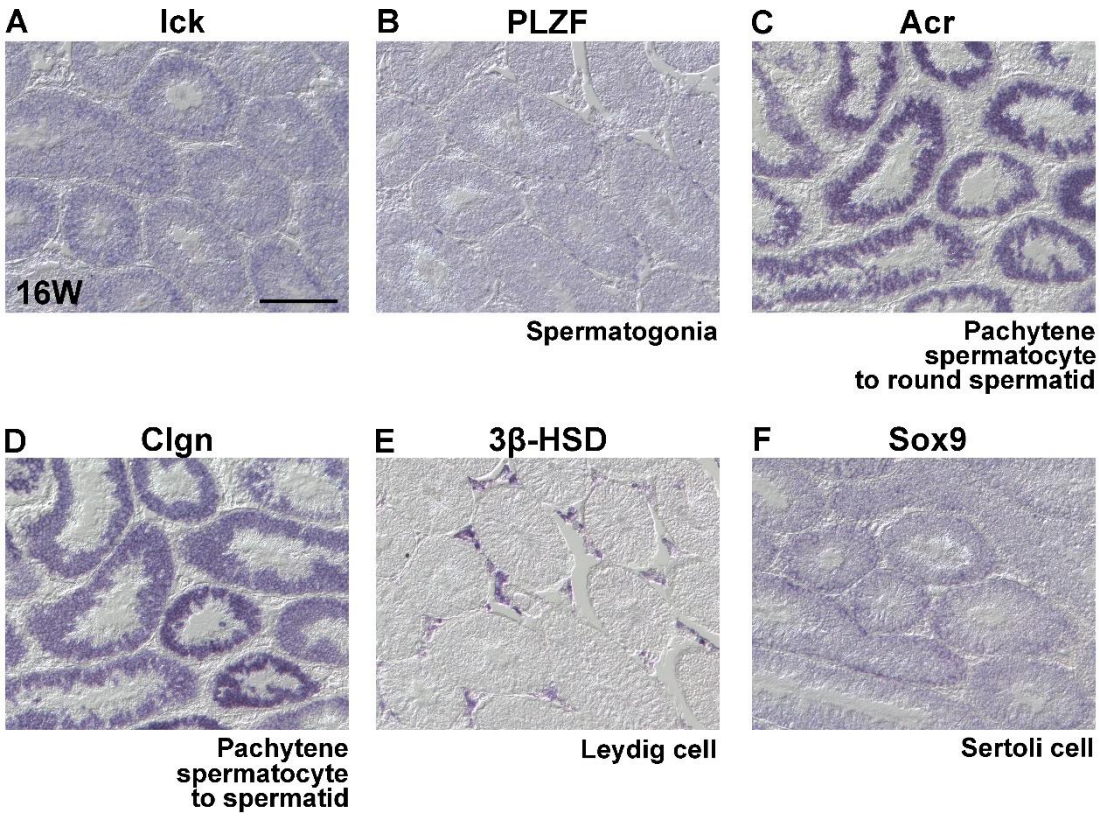

Figure 3. *Ick* expression in the adult testis.

(**A-F**) *In situ* hybridization analysis of mouse testicular sections at 16 wks, using probes against *Ick* (**A**), *PLZF* (a spermatogonia marker) (**B**), *Acr* (a pachytene spermatocyte to round spermatid marker) (**C**), *Clgn* (a pachytene spermatocyte to spermatid marker) (**D**), *3β-HSD* (a Leydig cell marker) (**E**), and *Sox9* (a Sertoli cell marker) (**F**). The *Ick* expression pattern was similar to that of *Acr* or *Clgn*. Scale bar, 200 μm.

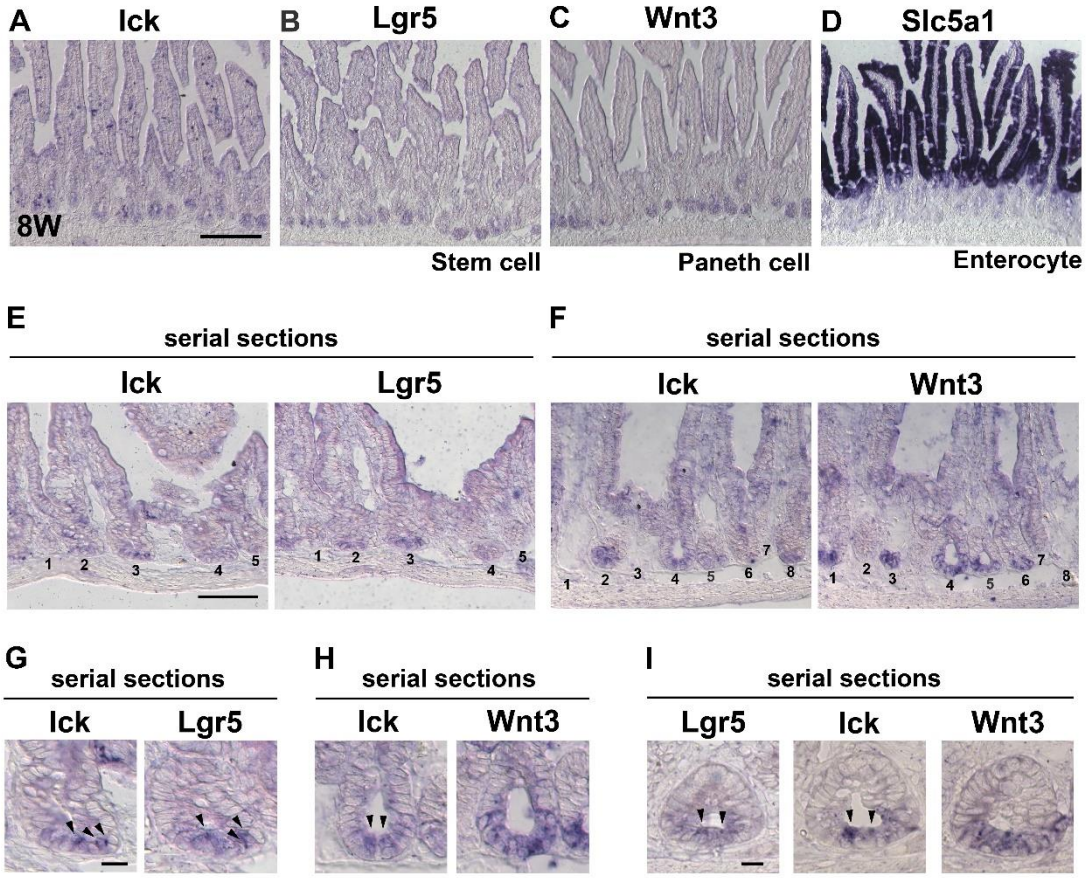

Figure 4. *Ick* expression in the adult intestine.

(**A-D**) *In situ* hybridization analysis of mouse small intestinal sections at 8 wks, using probes against *Ick* (**A**), *Lgr5* (an intestinal stem cell marker) (**B**), *Wnt3* (a Paneth cell marker) (**C**), and *Slc5a1* (an enterocyte marker) (**D**). (**E-I**) *In situ* hybridization analysis of serial sections from the mouse small intestine at 8 wks, using probes against *Ick*, *Lgr5*, and *Wnt3*. The numbers indicating each intestinal crypt in left panels correspond to those in right panels (**E**, **F**). (**G**) and (**H**) are higher magnification views of the crypt number 3 in (**E**) and the crypt number 4 in (**F**), respectively. *Ick* and *Lgr5* signals were enriched and overlapped in the inside of crypt bottoms (arrowheads). Scale bars, 100 μm (**A-D**), 50 μm (**E**, **F**), 10 μm (**G**, **H**, **I**).

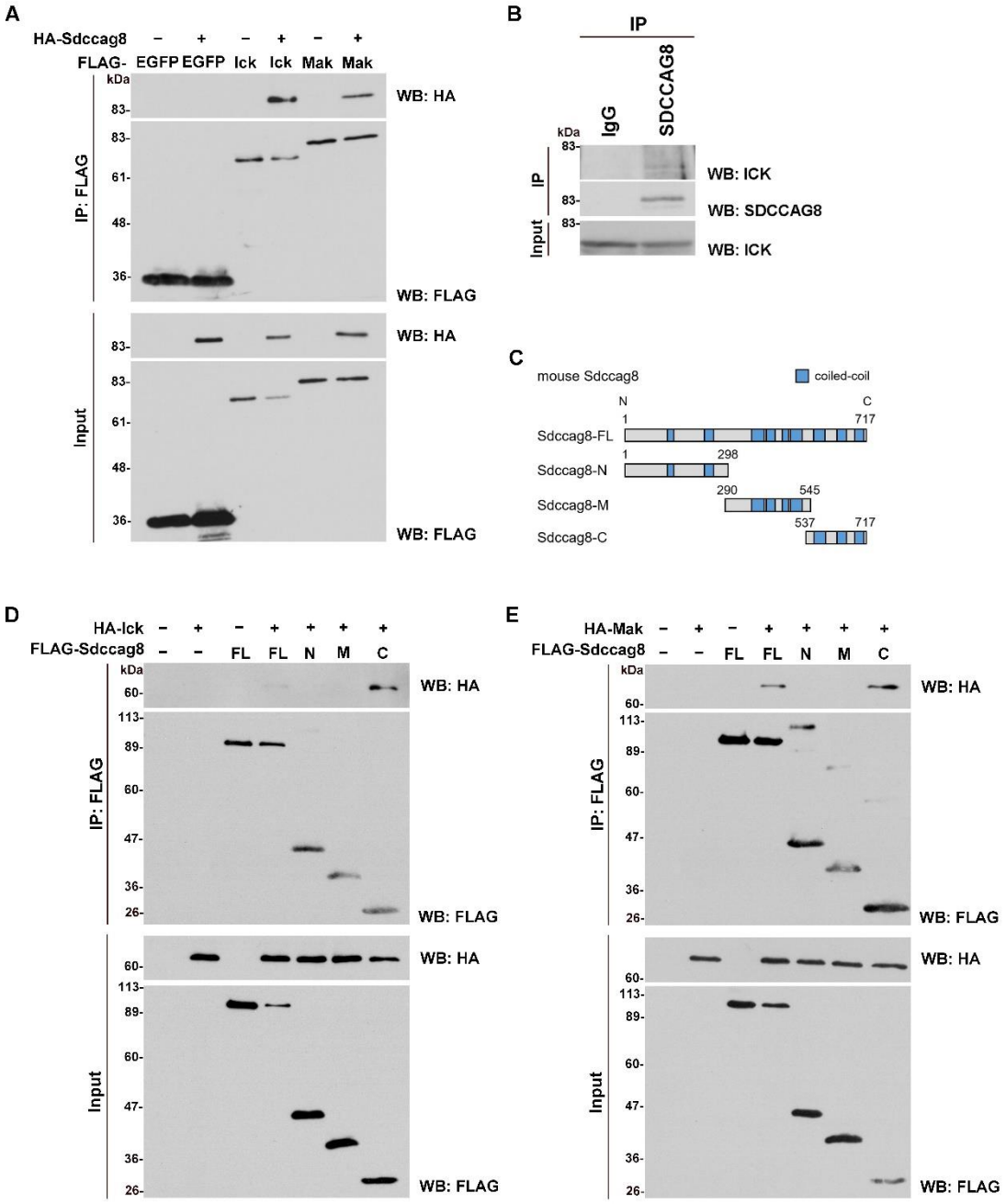

Figure 5. Interaction of Sdccag8 with Ick and Mak.

(**A**) Immunoprecipitation analysis of Sdccag8 and EGFP, Ick or Mak. Plasmids expressing FLAG-tagged EGFP, Ick or Mak, and HA-tagged Sdccag8 were co-transfected into HEK293T cells. The cell lysates were subjected to immunoprecipitation with an anti-FLAG antibody. Immunoprecipitated proteins were detected by Western blot analysis

with anti-FLAG and anti-HA antibodies.

(**B**) Immunoprecipitation was performed using HEK293T cells with an anti-SDCCAG8 antibody or isotype control. The ICK protein immunoprecipitated with the SDCCAG8 protein was detected by western blot analysis using an anti-ICK antibody.

(**C**) Schematic diagrams of mouse Sdccag8-FL, -N, -M, and -C.

(**D**, **E**) Immunoprecipitation analysis of Sdccag8-FL, -N, -M, or -C and Ick (D) or Mak (E). The plasmids expressing FLAG-tagged Sdccag8-FL, -N, -M, or -C, and HA-tagged Ick or Mak were co-transfected into HEK293T cells. The cell lysates were subjected to immunoprecipitation with an anti-FLAG antibody. Immunoprecipitated proteins were detected by Western blot analysis with anti-FLAG and anti-HA antibodies.

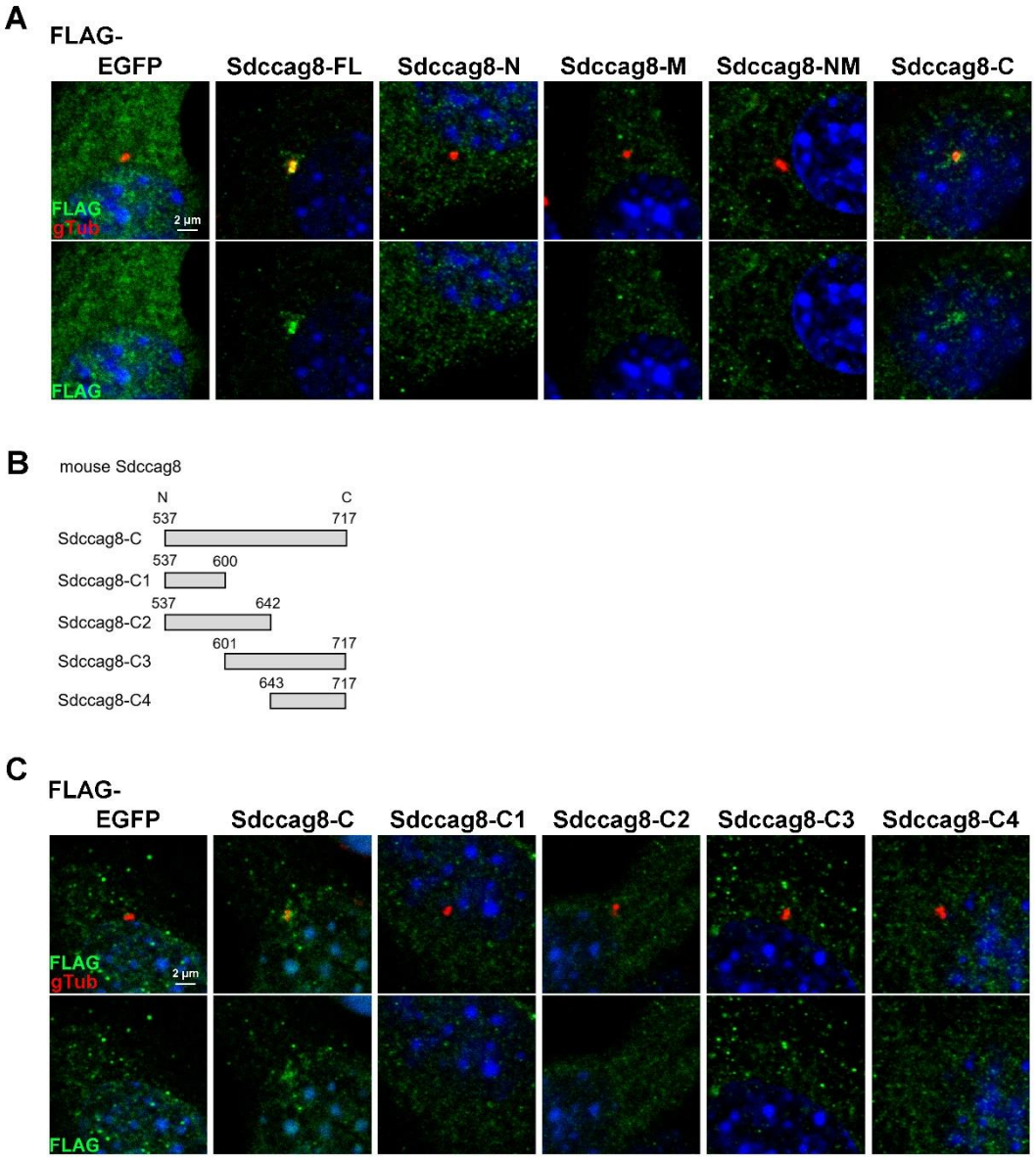

Figure 6. Roles of the C-terminal region in the localization of Sdccag8 to the centrosome in cultured cells.

(**A**) Plasmids expressing a FLAG-tagged EGFP, Sdccag8-FL, Sdccag8-N, Sdccag8-M, Sdccag8-NM, or Sdccag8-C were transfected into NIH-3T3 cells. Cells were immunostained with anti-FLAG and anti-γ-tubulin (gTub, a marker for centrosomes and basal bodies) antibodies. Nuclei were stained with DAPI (blue).

(**B**) Schematic diagrams of mouse Sdccag8-C, -C1, -C2, -C3, and -C4.

(**C**) Plasmids expressing a FLAG-tagged EGFP, Sdccag8-C, Sdccag8-C1, Sdccag8-C2, Sdccag8-C3, or Sdccag8-C4 were transfected into NIH-3T3 cells. Cells were immunostained with anti-FLAG and anti-γ-tubulin antibodies. Nuclei were stained with DAPI (blue).

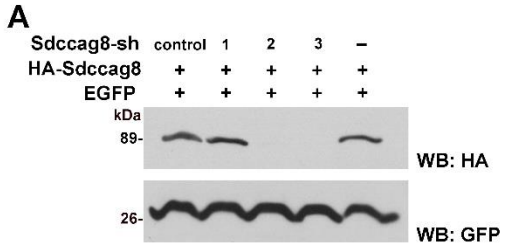
A
Sdccag8-sh control 1 2 3 –
HA-Sdccag8 + + + + +
EGFP + + + + +
kDa
89-
WB: HA
26-
WB: GFP

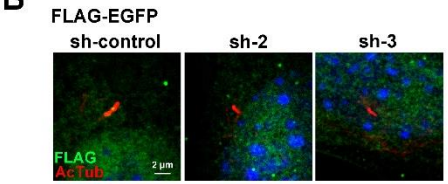
B
FLAG-EGFP
sh-control
sh-2
sh-3
FLAG
AcTub
2 μm

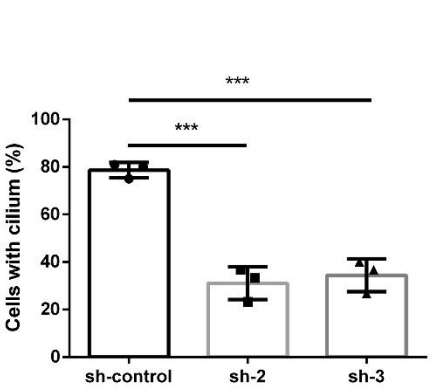
C
***
***
Cells with cilium (%)
100
80
60
40
20
0
sh-control
sh-2
sh-3

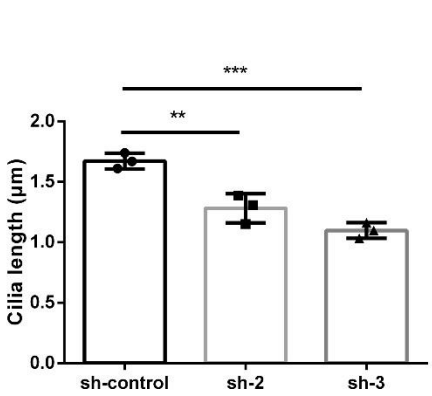
D
***
**
Cilia length (μm)
2.0
1.5
1.0
0.5
0.0
sh-control
sh-2
sh-3

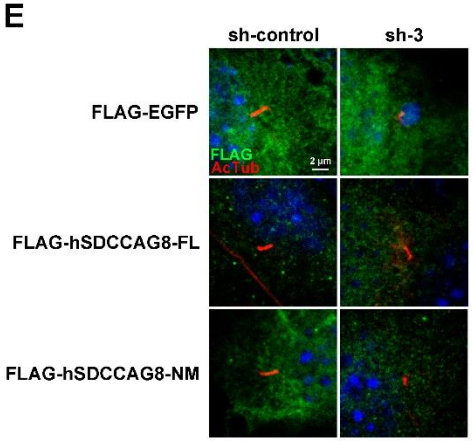
E
sh-control
sh-3
FLAG-EGFP
FLAG-hSDCCAG8-FL
FLAG-hSDCCAG8-NM
FLAG
AcTub
2 μm

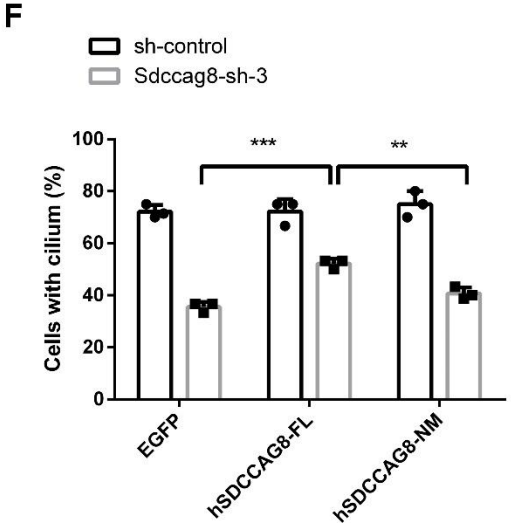
F
sh-control
Sdccag8-sh-3
***
**
Cells with cilium (%)
100
80
60
40
20
0
EGFP
hSDCCAG8-FL
hSDCCAG8-NM

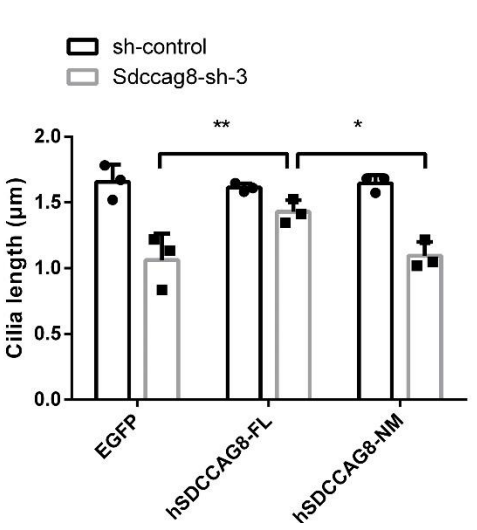
G
sh-control
Sdccag8-sh-3
**
*
Cilia length (μm)
2.0
1.5
1.0
0.5
0.0
EGFP
hSDCCAG8-FL
hSDCCAG8-NM

Figure 7. Roles of the C-terminal region of SDCCAG8 in cilia formation in cultured cells.

(**A**) Inhibition efficacy of shRNA expression constructs for *Sdccag8* knockdown. ShRNA-control, Sdccag8-shRNA1, Sdccag8-shRNA2, or Sdccag8-shRNA3 expression plasmids were co-transfected with plasmids expressing a HA-tagged Sdccag8 and a GFP into HEK293T cells. Western blot analysis was performed using anti-HA and anti-GFP antibodies. GFP was used as an internal transfection control. Sdccag8-shRNA2 and shRNA3 effectively suppressed Sdccag8 expression.

(**B**-**D**) ShRNA-control, Sdccag8-shRNA2, or Sdccag8-shRNA3 expression plasmids were co-transfected with a plasmid expressing FLAG-tagged EGFP into NIH-3T3 cells. Cells were immunostained with anti-FLAG and anti-acetylated α-tubulin (Actub, a ciliary marker) antibodies. Nuclei were stained with DAPI (blue) (B). The numbers (C) and length (D) of the cilia stained with an antibody against acetylated α-tubulin were measured. Sdccag8-shRNA2 and -shRNA3 inhibited ciliary formation. For the subsequent rescue experiment, Sdccag8-shRNA3 was used. Error bars show SD. $^{**}p < 0.01$, $^{***}p < 0.001$ (one-way ANOVA followed by Tukey's multiple comparisons test), n = 3.

(**E**-**G**) ShRNA-control or Sdccag8-shRNA3 expression plasmids were co-transfected into NIH-3T3 cells with plasmids expressing FLAG-tagged EGFP, hSDCCAG8-FL or hSDCCAG8-NM. Cells were immunostained with anti-FLAG and anti-acetylated α-tubulin antibodies. Nuclei were stained with DAPI (blue) (E). The numbers (F) and length (G) of the cilia stained with an antibody against acetylated α-tubulin were measured. Error bars show SD. $^{*}p < 0.05$, $^{**}p < 0.01$, $^{***}p < 0.001$ (two-way ANOVA followed by Tukey's multiple comparisons test), n = 3.

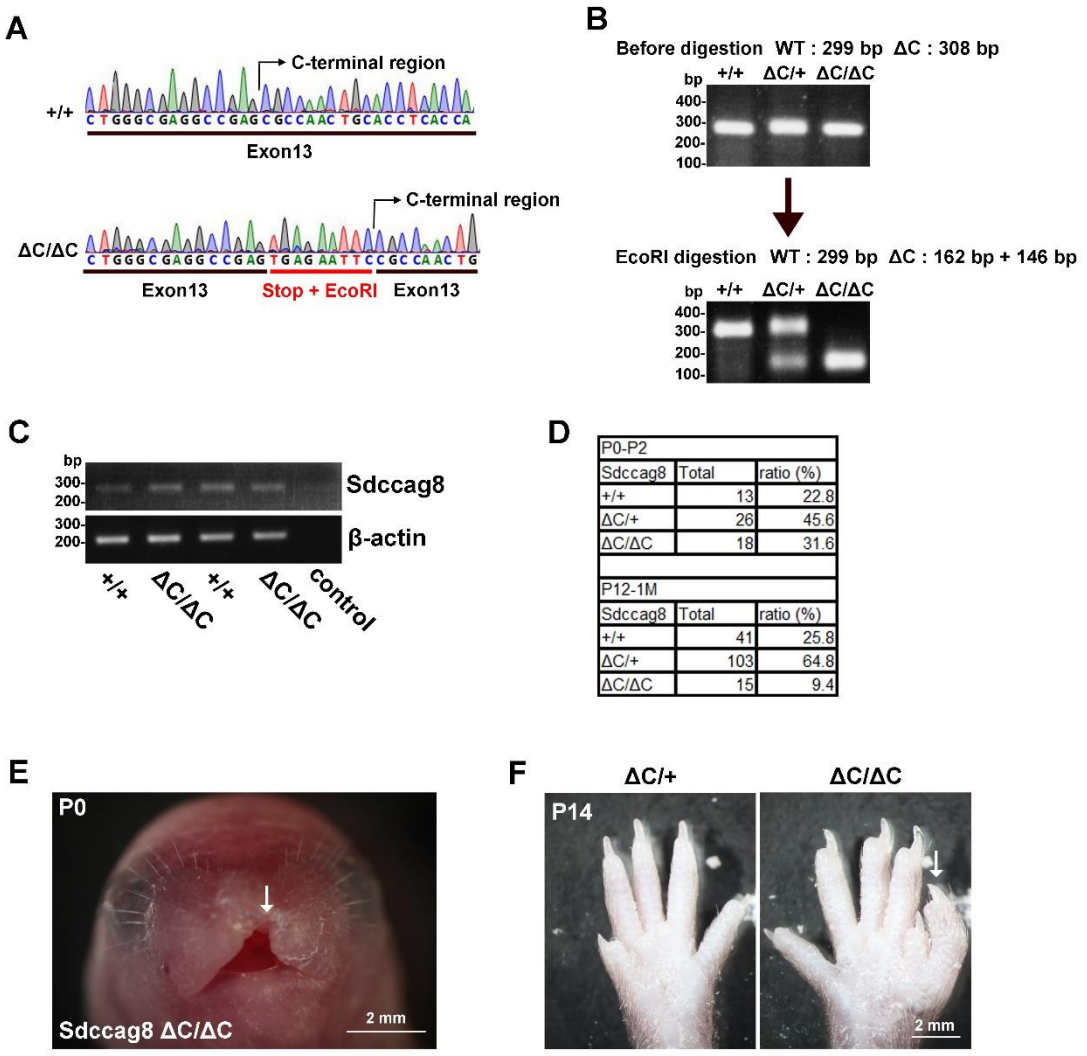

Figure 8. Generation and characterization of *Sdccag8*$^{\Delta C/\Delta C}$ mice.

(**A**) DNA sequences encoding around the Sdccag8 C-terminal region of *Sdccag8*$^{+/+}$ and *Sdccag8*$^{\Delta C/\Delta C}$ mice. The Arg537Stop codon and EcoRI restriction site were underlined in red. The Arg537Stop codon and EcoRI restriction site were knocked-in before Sdccag8-C (537–717 aa) in *Sdccag8*$^{\Delta C/\Delta C}$ mice.

(**B**) PCR analysis of Sdccag8 from tail tips of *Sdccag8*$^{+/+}$, *Sdccag8*$^{\Delta C/+}$, and *Sdccag8*$^{\Delta C/\Delta C}$ mice. The PCR products from *Sdccag8*$^{\Delta C/+}$ and *Sdccag8*$^{\Delta C/\Delta C}$ mice were able to be digested by EcoRI.

(**C**) RT-PCR analysis of *Sdccag8* (Exons 11-13) and *β-actin* in MEFs from *Sdccag8*$^{+/+}$

and *Sdccag8*$^{\Delta C/\Delta C}$ mice. *β-actin* was used as a loading control. *Sdccag8* mRNA was detected in *Sdccag8*$^{\Delta C/\Delta C}$ mice.

(**D**) Genotype distribution of the offspring from *Sdccag8*$^{\Delta C/+}$ parents at P0-2 and P12-1M.

(**E**, **F**) Skeletal defects in *Sdccag8*$^{\Delta C/\Delta C}$ mice. Gross appearance of the *Sdccag8*$^{\Delta C/\Delta C}$ face at P0 (E) and digits (F) in *Sdccag8*$^{\Delta C/+}$ and *Sdccag8*$^{\Delta C/\Delta C}$ mice at P14. Arrows indicate the cleft palate (E) and polydactyly (F) in *Sdccag8*$^{\Delta C/\Delta C}$ mice.

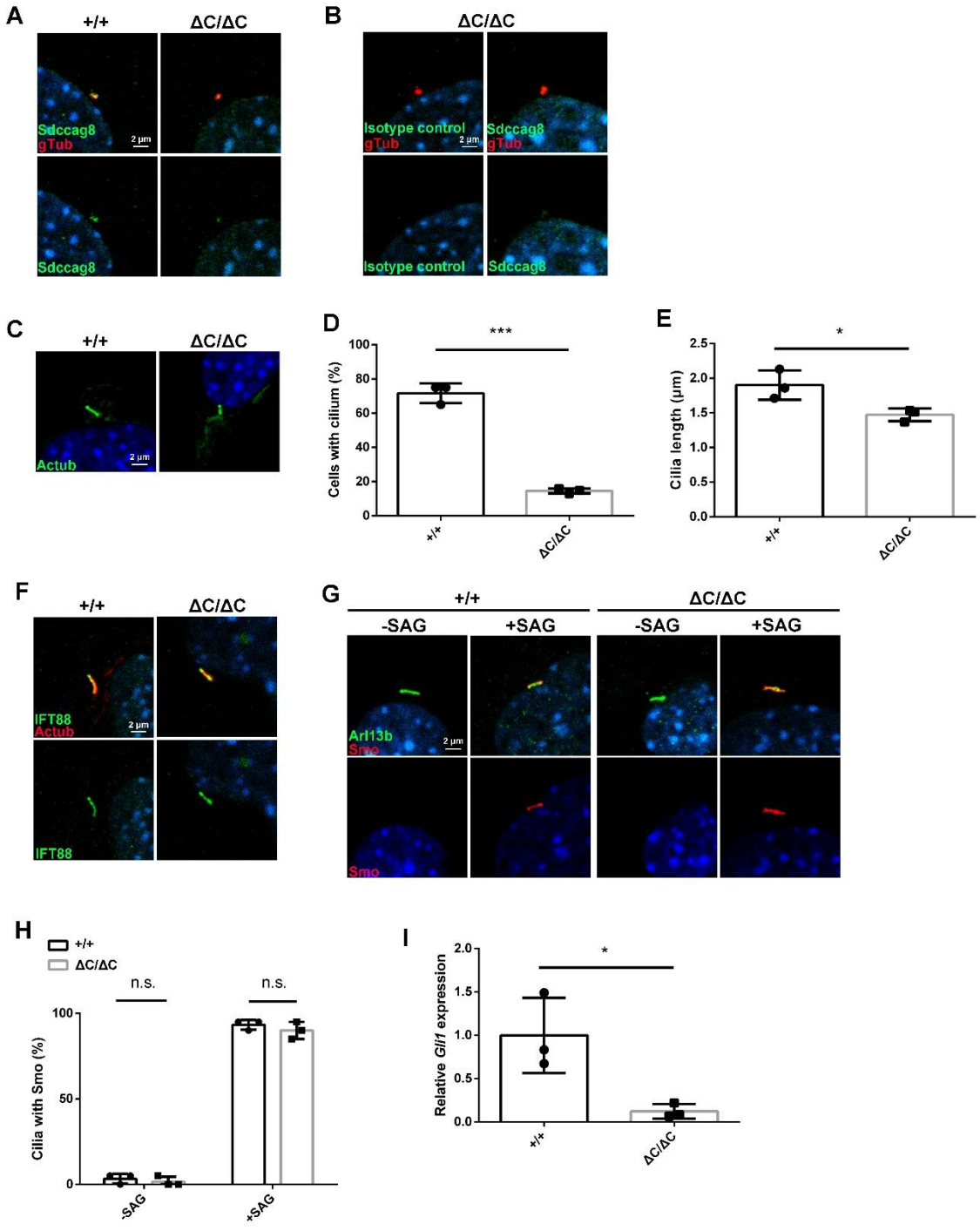

Figure 9. Ciliary defects in *Sdccag8*$^{\Delta C/\Delta C}$ MEFs.

(**A**) Immunofluorescent analysis of MEFs from *Sdccag8*$^{+/+}$ and *Sdccag8*$^{\Delta C/\Delta C}$ mice using anti-Sdccag8 and anti-γ-tubulin antibodies. Nuclei were stained with DAPI (blue).

(**B**) Immunofluorescent analysis of MEFs from *Sdccag8*$^{\Delta C/\Delta C}$ mice using isotype control, anti-Sdccag8 and anti-γ-tubulin antibodies. Nuclei were stained with DAPI (blue).

(**C-E**) Immunofluorescent analysis of MEFs from *Sdccag8*$^{+/+}$ and *Sdccag8*$^{\Delta C/\Delta C}$ mice using an anti-acetylated α-tubulin antibody. Nuclei were stained with DAPI (blue) (C). The numbers (D) and length (E) of the cilia stained with an antibody against acetylated α-tubulin were measured. Error bars show SD. *$p < 0.05$, ***$p < 0.001$ (unpaired t-test), n = 3 mice per genotype.

(**F**) Immunofluorescent analysis of MEFs from *Sdccag8*$^{+/+}$ and *Sdccag8*$^{\Delta C/\Delta C}$ mice using anti-IFT88 (a component of IFT complex) and anti-acetylated α-tubulin antibodies. Nuclei were stained with DAPI (blue).

(**G**, **H**) Immunofluorescent analysis of Smo agonist (SAG) treated or untreated MEFs from *Sdccag8*$^{+/+}$ and *Sdccag8*$^{\Delta C/\Delta C}$ mice using anti-Arl13b (a ciliary marker) and anti-Smo antibodies. Nuclei were stained with DAPI (blue) (G). The numbers of the Smo-positive cilia stained with an antibody against Arl13b were measured (H). Error bars show SD. n.s., not significant (unpaired t-test), n = 3 mice per genotype.

(**I**) qRT-PCR analysis of *Gli1* mRNA level in SAG-treated MEFs from *Sdccag8*$^{+/+}$ and *Sdccag8*$^{\Delta C/\Delta C}$ mice. Shh signal-dependent expression of *Gli1* was defective in the *Sdccag8*$^{\Delta C/\Delta C}$ MEF. Error bars show SD. *$p < 0.05$, (unpaired t-test), n = 3 mice per genotype.

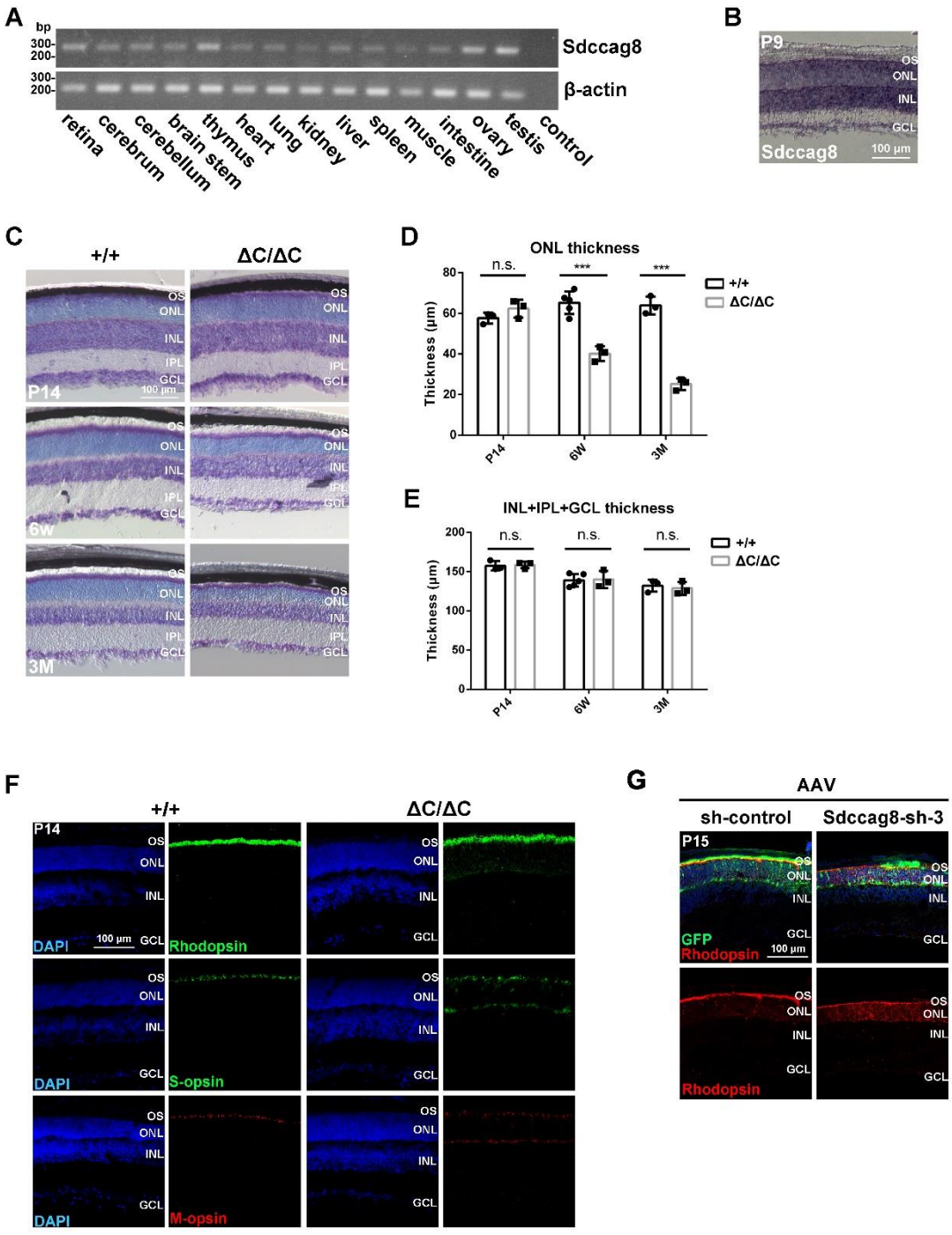

Figure 10. Photoreceptor degeneration in the *Sdccag8*$^{\Delta C/\Delta C}$ retina.

(**A**) RT-PCR analysis of *Sdccag8* (Exons 1-3) and *β-actin* in various mouse tissues at 4 wks. *β-actin* was used as a loading control. *Sdccag8* was ubiquitously expressed in a variety of tissues.

(**B**) *In situ* hybridization analysis of mouse retinal sections at P9, using a probe against *Sdccag8*. *Sdccag8* signals were detected in the ONL at P9.

(**C-E**) Toluidine blue staining of retinal sections from *Sdccag8*$^{+/+}$ and *Sdccag8*$^{\Delta C/\Delta C}$ mice at P14, 6 wks, and 3M (C). The ONL (D) and INL+IPL+GCL (E) thicknesses were measured. The ONL thickness progressively decreased in the *Sdccag8*$^{\Delta C/\Delta C}$ retina. Error bars show SD. ***$p < 0.001$, n.s., not significant (unpaired *t*-test). *Sdccag8*$^{+/+}$ at P14 and 3M, n = 3 mice; *Sdccag8*$^{+/+}$ at 6wks, n = 5 mice; *Sdccag8*$^{\Delta C/\Delta C}$ at P14, 6 wks, and 3M, n = 3 mice.

(**F**) Immunofluorescent analysis of retinal sections from *Sdccag8*$^{+/+}$ and *Sdccag8*$^{\Delta C/\Delta C}$ mice at P14 using antibodies as follows: anti-Rhodopsin (a marker for rod outer segments), anti-S-opsin (a marker for S-cone outer segments), and anti-M-opsin (a marker for M-cone outer segments). Nuclei were stained with DAPI (blue).

(**G**) Immunofluorescent analysis of retinal sections from mice injected with AAV-shRNA-control or AAV-Sdccag8-shRNA3 at P15 using anti-GFP and anti-Rhodopsin antibodies. The infected cells express AcGFP. Nuclei were stained with DAPI (blue).

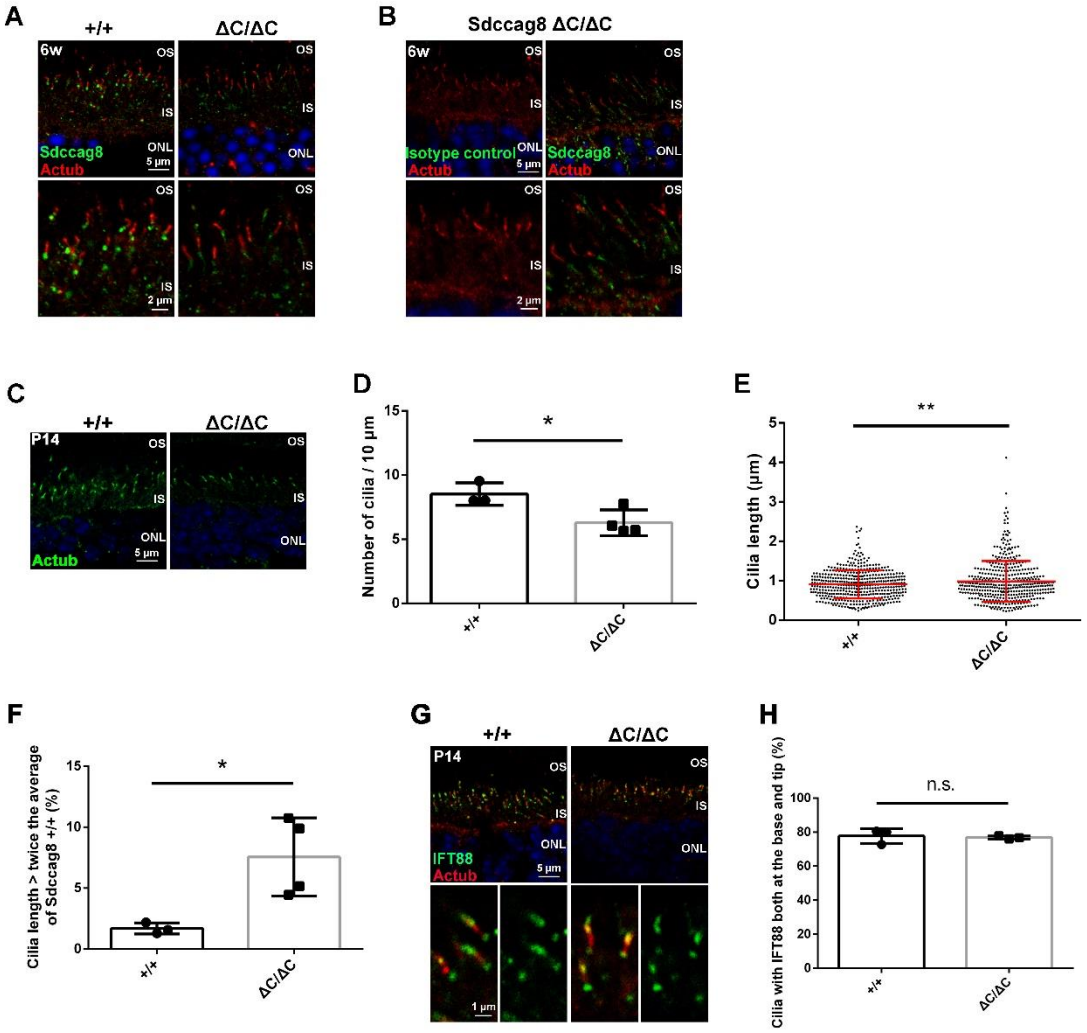

Figure 11. Abnormal cilia formation in *Sdccag8*$^{\Delta C/\Delta C}$ photoreceptor cells.

(**A**) Immunofluorescent analysis of retinal sections from *Sdccag8*$^{+/+}$ and *Sdccag8*$^{\Delta C/\Delta C}$ mice at 6 wks using anti-Sdccag8 and anti-acetylated α-tubulin antibodies. The lower panels indicate higher magnification views of the upper panels. Nuclei were stained with DAPI (blue).

(**B**) Immunofluorescent analysis of retinal sections from *Sdccag8*$^{\Delta C/\Delta C}$ mice at 6 wks using isotype control, anti-Sdccag8 and anti-γ-tubulin antibodies. The lower panels indicate higher magnification views of upper panels. Nuclei were stained with DAPI (blue).

(**C**-**E**) Immunofluorescent analysis of retinal sections from *Sdccag8*$^{+/+}$ and *Sdccag8*$^{\Delta C/\Delta C}$ mice at P14 using the anti-acetylated α-tubulin antibody. Nuclei were stained with DAPI (blue) (C). The numbers (D) and length (E) of the cilia stained with an antibody against acetylated α-tubulin were measured. Error bars show SD. *$p < 0.05$, **$p < 0.01$ (unpaired t-test). (D) *Sdccag8*$^{+/+}$, n = 3 mice; *Sdccag8*$^{\Delta C/\Delta C}$, n = 4 mice. (E) *Sdccag8*$^{+/+}$, n = 465 cilia from 3 mice; *Sdccag8*$^{\Delta C/\Delta C}$, n = 427 cilia from 4 mice.

(**F**) Comparison of the percentage of cilia longer than twice the average of the photoreceptor cilia length of the *Sdccag8*$^{+/+}$ retina between the *Sdccag8*$^{+/+}$ and *Sdccag8*$^{\Delta C/\Delta C}$ retina at P14. The length of the cilia stained with an antibody against acetylated α-tubulin were measured. Error bars show SD. *$p < 0.05$ (unpaired t-test). *Sdccag8*$^{+/+}$, n = 3 mice; *Sdccag8*$^{\Delta C/\Delta C}$, n = 4 mice.

(**G, H**) Immunofluorescent analysis of retinal sections from *Sdccag8*$^{+/+}$ and *Sdccag8*$^{\Delta C/\Delta C}$ mice at P14 using anti-IFT88 and anti-acetylated α-tubulin antibodies. The lower panels show higher magnification views of the upper panels. Nuclei were stained with DAPI (blue) (G). The numbers of the cilia with IFT88 both at the base and tip were measured (H). Error bars show SD. n.s., not significant (unpaired t-test), n = 3 mice per genotype. OS, outer segments; IS, inner segments; ONL, outer nuclear layer; INL, inner nuclear layer; GCL, ganglion cell layer.

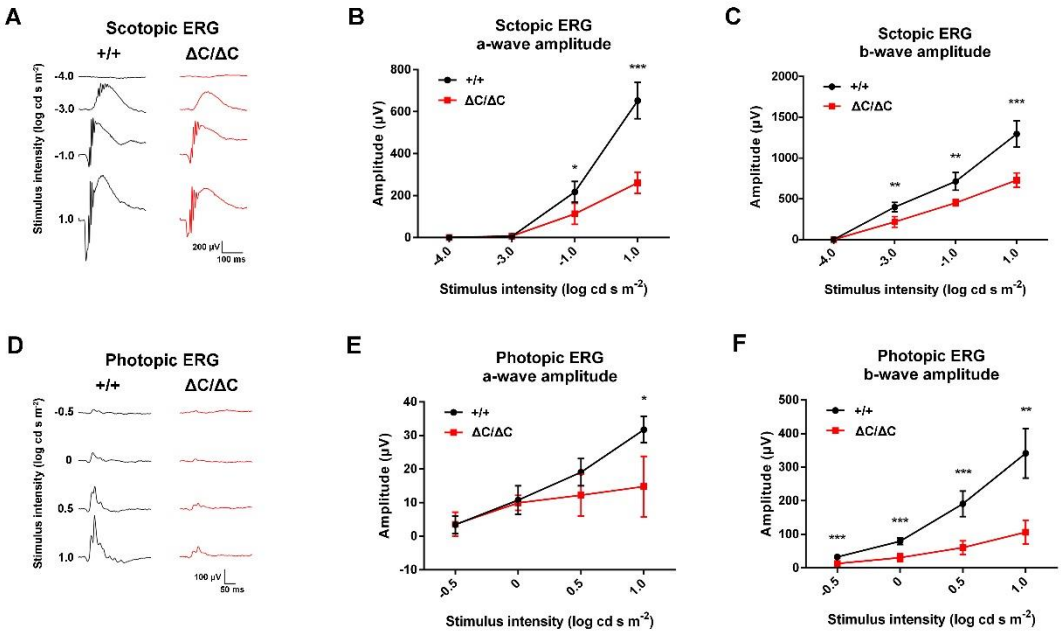

Figure 12. Reduction of ERG activities in *Sdccag8*$^{\Delta C/\Delta C}$ mice.

(**A-F**) ERG analysis of *Sdccag8*$^{+/+}$ and *Sdccag8*$^{\Delta C/\Delta C}$ mice at 6 wks. (A, D) Representative scotopic ERGs (A) elicited by four different stimulus intensities (−4.0 to 1.0 log cd s/m^2) and photopic ERGs (D) elicited by four different stimulus intensities (−0.5 to 1.0 log cd s/m^2) from *Sdccag8*$^{+/+}$ and *Sdccag8*$^{\Delta C/\Delta C}$ mice. (B, C) The scotopic amplitudes of a- (B) and b-waves (C) are shown as a function of the stimulus intensity. (E, F) The photopic amplitudes of a- (E) and b-waves (F) are shown as a function of the stimulus intensity. Error bars show SD. *$p < 0.05$, **$p < 0.01$, ***$p < 0.001$ (unpaired t-test). *Sdccag8*$^{+/+}$, n = 6 mice; *Sdccag8*$^{\Delta C/\Delta C}$, n = 3 mice.

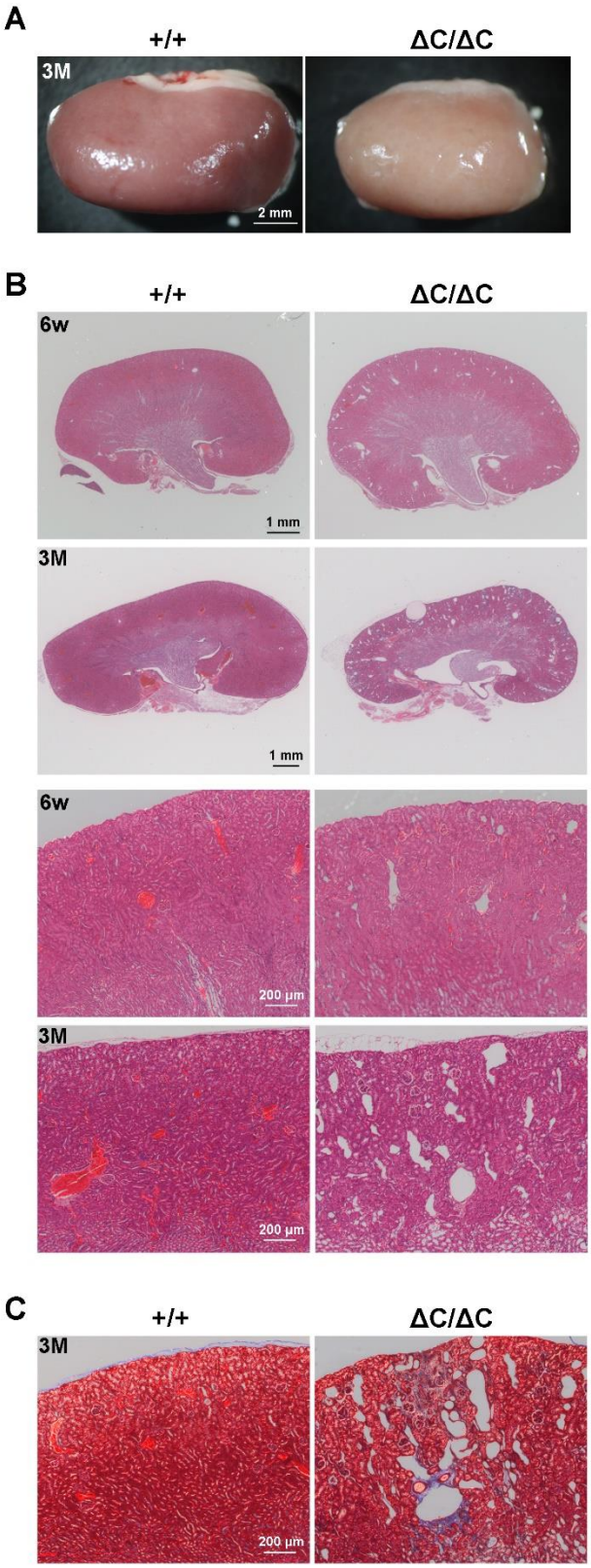

Figure 13. Renal degeneration in the *Sdccag8*$^{\Delta C/\Delta C}$ kidney.

(**A**) Gross appearance of kidneys from *Sdccag8*$^{+/+}$ and *Sdccag8*$^{\Delta C/\Delta C}$ mice at 3M. Pale appearance was observed in the *Sdccag8*$^{\Delta C/\Delta C}$ kidney.

(**B**) H&E staining of renal sections from *Sdccag8*$^{+/+}$ and *Sdccag8*$^{\Delta C/\Delta C}$ mice at 6 wks and 3M. The lower panels indicate higher magnification views of each upper panels. Progressive cyst formation was observed in the *Sdccag8*$^{\Delta C/\Delta C}$ kidney.

(**C**) Masson trichrome staining of renal sections from *Sdccag8*$^{+/+}$ and *Sdccag8*$^{\Delta C/\Delta C}$ mice at 3M. Interstitial fibrosis was observed in the *Sdccag8*$^{\Delta C/\Delta C}$ kidney.

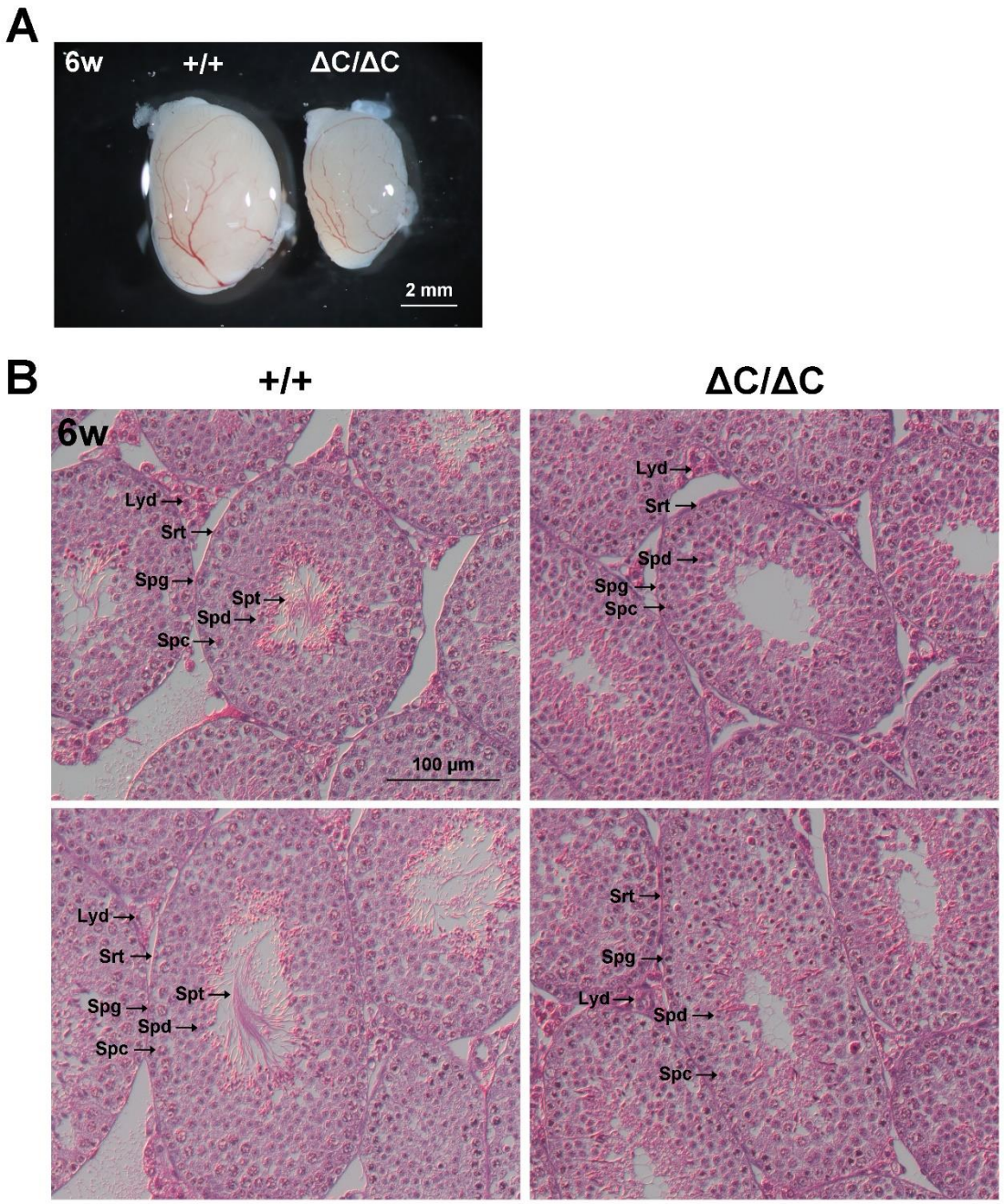

Figure 14. Abnormal spermatogenesis in the *Sdccag8*$^{\Delta C/\Delta C}$ testis.

(**A**) Gross appearance of the testes of male *Sdccag8*$^{+/+}$ and *Sdccag8*$^{\Delta C/\Delta C}$ mice at 6 wks. The testes from *Sdccag8*$^{\Delta C/\Delta C}$ mice were smaller than those from *Sdccag8*$^{+/+}$ mice.

(**B**) H&E staining of testicular sections from male *Sdccag8*$^{+/+}$ and *Sdccag8*$^{\Delta C/\Delta C}$ mice at 6wks. Mature sperm could not be observed in the *Sdccag8*$^{\Delta C/\Delta C}$ testis.

Spg, spermatogonia; Spc, spermatocytes; Spd, spermatids; Spt, sperm tails; Lyd, Leydig cells; Srt, Sertoli cells.

Table 1. Identification of proteins interacting with Ick protein by yeast two-hybrid screening.

Gene	Symbol
Coiled-coil domain containing 136	Ccdc136
Coiled-coil domain containing 159	Ccdc159
Coiled-coil domain containing 85c	Ccdc85c
Centralsommal protein 250	Cep250
Compartment of oligomeric golgi complex6	Cog6
Cleavage and polyadenylation specific factor	Cpsf6
Exosome component 8	Exosc8
Internexin neuronal intermediate filament protein, alpha	Ina
Myosin phosphatase Rho interacting protein	Mprip
Neural precursor cell expressed, developmentally down regulated 4	Nedd4
Pryurate kinase, muscle	Pkm
Periphilin 1	Pphln1
Proteasome 26S subunite 1	Psmc1
Proteasome 26S subunite 6	Psmc6
Rab11 family interacting protein 4	Rab11fip4
Serologically colon cancer antigen 8	Sdccag8
SWI/SNF related, matrix associated, actin dependent regulator of chromatin subfamily c, member 2	Smarcc2
Sorting nexin 29	Snx29
Sperm flagellar 1	Spef1
Single-strand DNA binding protein 2	Ssbp2
Tripartite motif containing 27	Trim27
TRIO and F-actin binding protein	Triobp
Vimentin	Vim

Table 2. Primer sequences.

Experiments	Primer name	Sequence (5' to 3')
Constructs		
pCAGGSII-FLAG/HA-mMak	mMak-ORF-Xho1-51	TTTCTCGAGATGAACCGATACACAACCATGAAGCAG
	mMak-ORF-Not1-31	TTTGCGGCCGCCTACCGGTGGCCTCCATACTTAGCCA
pCAGGSII-FLAG/HA-mSdccag8-FL	mSdccag8-ORF-51	GCTCGAGATGGCGAAGTCCCCAGGGAACTCTAC
	mSdccag8-ORF-31	GGCGGCCGCTCAGCAATCAGATTGTGGCATGCTG
pCAGGSII-FLAG-mSdccag8-N	mSdccag8-ORF-51	GCTCGAGATGGCGAAGTCCCCAGGGAACTCTAC
	mSdccag8-N-terminal-32	GGCGGCCGCTCAGGAAAGAACAGCTTCATGCTGAGCAC
pCAGGSII-FLAG-mSdccag8-M	mSdccag8-middle-51	GCTCGAGTGTGCTCAGCATGAAGCTGTTCTTTC
	mSdccag8-middle-32	GGCGGCCGCTCATTCCAGTCTGGTGAGGTGCAGTTGGC
pCAGGSII-FLAG-mSdccag8-NM	mSdccag8-ORF-51	GCTCGAGATGGCGAAGTCCCCAGGGAACTCTAC
	mSdccag8-middle-32	GGCGGCCGCTCATTCCAGTCTGGTGAGGTGCAGTTGGC
pCAGGSII-FLAG-mSdccag8-C	mSdccag8-C-terminal-51	GCTCGAGCGCCAACTGCACCTCACCAGACTGGA
	mSdccag8-ORF-31	GGCGGCCGCTCAGCAATCAGATTGTGGCATGCTG
pCAGGSII-FLAG-mSdccag8-C1	mSdccag8-C-terminal-51	GCTCGAGCGCCAACTGCACCTCACCAGACTGGA
	mSdccag8-middle1-31	TTTGCGGCCGCTCACAGAAATGTGTTCTGGGATGTCAGCA
pCAGGSII-FLAG-mSdccag8-C2	mSdccag8-C-terminal-51	GCTCGAGCGCCAACTGCACCTCACCAGACTGGA
	mSdccag8-middle2-31	TTTGCGGCCGCTCATAACTTCTCTAGCTTGTCACACAAGT
pCAGGSII-FLAG-mSdccag8-C3	mSdccag8-C-terminal1-51	GGGCTCGAGACAAAATTAAAAGAAGAATGCTGCT
	mSdccag8-ORF-32	GGGGCGGCCGCTCAGCAATCAGATTGTGGCATGCTG
pCAGGSII-FLAG-mSdccag8-C4	mSdccag8-C-terminal2-51	GGGCTCGAGCAGAAGAGAAATGACGAACTAGAAG
	mSdccag8-ORF-32	GGGGCGGCCGCTCAGCAATCAGATTGTGGCATGCTG
pCAGGSII-FLAG-hSDCCAG8-FL	hSDCCAG8-ORF-XhoI-51	TTTCTCGAGATGGCGAAGTCCCCGGAGAACTCTAC
	hSDCCAG8-ORF-NotI-31	TTTGCGGCCGCTCAGCAATCAGATTGTGGCATGCTG
pCAGGSII-FLAG-hSDCCAG8-NM	hSDCCAG8-ORF-XhoI-51	TTTCTCGAGATGGCGAAGTCCCCGGAGAACTCTAC
	hSDCCAG8-middle-NotI-31	TTTGCGGCCGCTCATTCCTGTCTGGTGAGGTGCAGTTGGTG
pCAGGSII-HA-EGFP	EGFP-ORF-XhoI-51	TTTCTCGAGATGGTGAGCAAGGGCGAGGAGCTG
	EGFP-ORF-NotI-31	TTTGCGGCCGCTTACTTGTACAGCTCGTCCATGCCGAG
genotyping		
	mSdccag8-PCR-51	AATATGGGTTCTTTTCCTCCCTCTGTC
	mSdccag8-PCR-31	CCGTAATATGCCTGAAAGCTGTGTGTG
in situ hybridization		
	Lgr5-ISH-51	TGTCCTTGCTGGCGCTGCTGCAG
	Lgr5-ISH-31	AGACGGCCTGGGGAAGAGATGAG
	Slc5a1-ISH-51	ATCCTCGCCCTGTGGTACTGGTG
	Slc5a1-ISH-31	TGGTCCAGCCCACAGAACAGGTC
	Wnt3-ISH-51	CTGGCCCTGGGCCAGCAGTACAC
	Wnt3-ISH-31	AGGTGTGCACATCGTAGATGCGA
RT-PCR		
	β-actin-F	CGTGCGTGACATCAAAGAGAA
	β-actin-R	TGGATGCCACAGGATTCCAT
Exon1-3	mSdccag8-RT-PCR-51	ACCCTGGAGGACAGTCTGGGGCAATAC
	mSdccag8-RT-PCR-31	ACAACTTTCGTCTTCGCGGTGGAGATG
Exon11-13	mSdccag8-RT-PCR-52	CCACGTTGCGTCTCAGGAAATGGACGT
	mSdccag8-RT-PCR-33	CTCTGTGACTCGCAGGCACTCCTGTCT
qRT-PCR		
	Rpl4-F	GATATGCCATCTGTTCTGCCCT
	Rpl4-R	CTTGCCAGCTCTCATTCTCTGA
	Gli1-Q3	GCAGTGGGTAACATGAGTGTCT
	Gli1-Q4	AGGCACTAGAGTTGAGGAATTGT
AAV titration		
	pCAG-q-PCR-QF3	CCTGGCATTATGCCCAGTACATG
	pCAG-q-PCR-QR3	GCTCACCTCGACCATGGTAATAG